

ESTCP Cost and Performance Report

(UX-9812)



Electromagnetic Induction and Magnetic Sensor Fusion for Enhanced UXO Target Classification

February 2004



ENVIRONMENTAL SECURITY
TECHNOLOGY CERTIFICATION PROGRAM

U.S. Department of Defense

COST & PERFORMANCE REPORT

ESTCP Project: UX-9812

TABLE OF CONTENTS

	Page
1.0 EXECUTIVE SUMMARY	1
2.0 TECHNOLOGY DESCRIPTION	3
2.1 BACKGROUND AND INTENDED USE.....	3
2.2 TECHNOLOGY DESCRIPTION	3
2.2.1 Mobilization and Operational Requirements	6
2.2.2 Personnel and Training Requirements.....	7
2.2.3 Health and Safety Training.....	8
2.3 ADVANTAGES AND LIMITATIONS OF THE TECHNOLOGY.....	8
3.0 DEMONSTRATION DESIGN	9
3.1 PERFORMANCE OBJECTIVES	9
3.1.1 L Range Demonstration	9
3.1.2 BBR Impact Area Demonstration.....	9
3.2 SELECTION OF TEST SITES	10
3.3 TEST SITE HISTORY AND CHARACTERISTICS	11
3.3.1 L Range Demonstration	11
3.3.2 BBR Impact Area Demonstration.....	12
3.4 PHYSICAL SETUP AND OPERATION	14
3.4.1 L Range Demonstration	14
3.4.2 BBR Impact Area Demonstration.....	14
4.0 PERFORMANCE ASSESSMENT	17
4.1 L RANGE DEMONSTRATION.....	17
4.1.1 Remediation Results	17
4.1.2 Performance Data.....	18
4.1.3 Data Assessment.....	20
4.1.4 Technology Comparison.....	21
4.2 BBR IMPACT AREA SURVEY.....	23
4.2.1 Pre-Demonstration Measurements.....	23
4.2.2 Survey Data.....	26
4.2.3 Data Assessment.....	27
4.2.3.1 EM61 MkII Electronic and Calibration Issues	27
4.2.3.2 EM61 MkI Signal to Noise Ratios.....	29
4.2.3.3 EM61 Model Fits.....	31
4.2.3.4 An Alternate Discrimination Approach.....	33
4.2.3.5 Technology Comparison.....	36

TABLE OF CONTENTS (continued)

		Page
5.0	COST ASSESSMENT	39
5.1	COST ANALYSIS.....	39
5.2	COST COMPARISON.....	40
6.0	REFERENCES	41
APPENDIX A	POINTS OF CONTACT.....	A-1
APPENDIX B	MTADS TARGET REPORT FROM THE L RANGE DEMONSTRATION	B-1
APPENDIX C	MTADS TARGET REPORT FROM THE BBR IMPACT AREA DEMONOSTRATION	C-1

FIGURES

		Page
Figure 1.	Direction and Magnitude of the Magnetic Field Transmitted by the MTADS EM61 Array	5
Figure 2.	Road Map Showing Location of the L Range.	11
Figure 3.	Aerial View of the Army Research Laboratory Blossom Point L Range with Approximate Location of the First Demonstration Highlighted.....	12
Figure 4.	A Portion of USGS 7.5-Minute Map with the Perimeter of the BBR Impact Area Shown in Red	13
Figure 5.	Aerial Photograph of Logistics Support for the Second Demonstration	15
Figure 6.	Example 81-mm Mortar and 60-mm Mortar Remediated at the L Range.....	17
Figure 7.	Example of Nonordnance Remediated at L Range.....	17
Figure 8.	Two-Dimensional Representation of the Three-Beta Fits for 81-mm Mortars in the Demonstration	18
Figure 9.	Two-Dimensional Representation of the Three-Beta Fits for Other Recovered Targets from the Demonstration Plotted as in Figure 8.....	19
Figure 10.	ROC Curve for the Detection of 81-mm Mortars	19
Figure 11.	ROC Curve for the Detection of All Ordnance	19
Figure 12.	Two-Dimensional Representation of Three Beta Fits for All Targets Dug in the Demonstration with Ellipses for Each Ordnance Class Derived from the 81-mm Mortar Ellipse.....	20
Figure 13.	Results of a Monte Carlo Simulation of Fitted Betas Resulting from a Range of Model 81-mm Mortars with Two Sources of Noise Compared to the Results from the First Demonstration.....	22
Figure 14.	ROC Curve for Classification Using These Methods Compared to Results Using Magnetic Dipole Size and Dipole Orientation	23
Figure 15.	Measured EM63 Response Profiles at Eight Time Gates from a Traverse over a Horizontal 105-mm Projectile 66 cm below the Sensor	24
Figure 16.	Measured EM63 Response Profiles at Eight Time Gates from a Traverse over a Frag Cluster.....	25
Figure 17.	Comparison of the Results of All Three Surveys of the Seeded Area in a Small Subgrid.....	26
Figure 18.	Comparison of the Signals from the EM61 MkII Array and the EM61 MkI Array Arising from a High-SNR 105-mm Projectile.....	28
Figure 19.	Comparison of the Signals from the EM61 MkII Array and the EM61 MkI Array Arising from a Low-SNR 105-mm Projectile	29
Figure 20.	Comparison of the Noise Observed with the EM61 MkI at Three Sites	30
Figure 21.	Power Spectral Density of the EM61 MkI Noise at Two Sites	30
Figure 22.	Plots of Primary Beta Versus Secondary Beta for Ordnance Items and Clutter....	31
Figure 23.	Data Fit and Chi-Square Contours for a High-SNR 155-mm Projectile	32
Figure 24.	Data Fit and Chi-Square Contours for a Low-SNR 155-mm Projectile.....	32
Figure 25.	Data Fit and Chi-Square Contours for a Frag Cluster.....	33
Figure 26.	Plots of Reduced Chi-Square Versus Peak Signal for Ordnance and Clutter.....	34
Figure 27.	Comparison of Beta Sphere Discriminant to Goodness-of-Fit Discriminant.	35

FIGURES (continued)

	Page
Figure 28. Results of the Constrained Fits	35
Figure 29. ROC Curves Comparing the Discrimination Performance of the Three Methods.....	36
Figure 30. ROC Curves Comparing the Discrimination Performance of the Constrained Beta Fit with the Two Magnetometry Analyses Used in this Demonstration	37

TABLES

	Page
Table 1. Typical Logistics Costs for a 2-Week Survey Assuming No Remediation.....	7
Table 2. Impact Area Survey Coordinates Provided by Ellsworth AFB	14
Table 3. Schedule for the L Range Demonstration.....	14
Table 4. Location of Emplaced Seed Targets at the BBR Impact Area.....	15
Table 5. Schedule for the BBR Impact Area Demonstration.....	16
Table 6. Size Distributions Used in Magnetometer Analysis of the Demonstration Results	22
Table 7. Gate Times for the Two Modes of the MTADS EM61 MkIIs	25
Table 8. Summary of the Magnetometer Analysis Results.....	26
Table 9. Cost Comparison for a Hypothetical 200-Acre Survey Using These Methods	39

ACRONYMS AND ABBREVIATIONS

AFB	Air Force Base
APG	Aberdeen Proving Ground
ARL	Army Research Laboratory
ATC	Aberdeen Test Center
BBR	Badlands Bombing Range, SD
CES	Civil Engineer Squadron
DAS	data analysis system
DoD	Department of Defense
EM	electromagnetic
EOD	explosives ordnance disposal
ERDC	Engineer Research and Development Center
ESTCP	Environmental Security Technology Certification Program
FA	false alarm
GIS	geographic information system
GPS	global positioning system
HAZWOPR	hazardous waste operations
IDA	Institute for Defense Analyses
JPG	Jefferson Proving Ground
ms	milliseconds
MTADS	Multi-Sensor Towed Array Detection System
NBS	National Bureau of Standards
NIST	National Institute of Standards and Technology
NRL	Naval Research Laboratory
OST	Oglala Sioux Tribe
PD	probability of detection
PNN	probabilistic neural net
QC	quality control

ACRONYMS AND ABBREVIATIONS (continued)

RMS	root mean square
ROC	receiver operating characteristic
RTK	real-time kinematic
SERDP	Strategic Environmental Research and Development Program
SNR	signal to noise ratio
S/N	signal to noise
USGS	U.S. Geological Survey
UXO	Unexploded Ordnance

ACKNOWLEDGEMENTS

The Multi-Sensor Towed Array Detection System (MTADS) development and initial demonstrations were supported by the Environmental Security Technology Certification Program (ESTCP) Program Office. This program, aimed to increase the classification ability of the MTADS system, was also supported by ESTCP.

The Naval Research Laboratory has managed all MTADS activities. The principal investigator for this program is Dr. H.H. Nelson. Dr. J. R. McDonald is the deputy principal investigator.

We wish to acknowledge the critically important contributions made by AETC, Inc. Tom Bell, Bruce Barrow, and Nagi Khadr were instrumental in the development of the model used in this program, and Bernard Puc modified the data analysis system to make use of these methods. We appreciate continual program administrative support by Richard Robertson (Hughes Associates) and field support by Larry Koppe (GeoCenters, Inc.) and Glenn Harbaugh (Nova Research, Inc.).

Finally, we wish to express our grateful appreciation to Dr. Jeff Marqusee for his unflagging and continual commitment to developing and refining automated UXO detection and remediation technologies. This commitment has led to demonstration and validation of a fully field-hardened prototype and to its transition to the commercial sector where it is currently available to provide commercial UXO services and continual improvements of our understanding and ability to make use of MTADS data.

Technical material contained in this report has been approved for public release.

This page left blank intentionally.

1.0 EXECUTIVE SUMMARY

Traditional methods for buried unexploded ordnance (UXO) detection, characterization, and remediation are labor-intensive, slow, and inefficient. A large portion, approaching 70% in some cases, of the total budget of a typical remediation effort is spent on digging targets that do not turn out to be UXO.

The Environmental Security Technology Certification Program (ESTCP), has supported the Naval Research Laboratory (NRL) in developing the Multi-Sensor Towed Array Detection System (MTADS), to address these deficiencies. It is efficient and simple to operate by relatively untrained personnel. It can detect and locate ordnance with accuracies on the order of 15 cm. However, even with careful mission planning and site-specific training, there are still significant numbers of nonordnance targets selected.

Most UXO fit a specific profile: they are long and slender with typical length-to-diameter aspect ratios of four or five. Many clutter items, on the other hand, do not fit this profile. Using electromagnetic (EM) pulsed-induction sensor data, we have developed a model-based estimation procedure that relies on exploiting the dependence of the induced field on target size, shape, and orientation to determine if a target is likely to be a UXO item.

These methods were the subject of two demonstrations. The first demonstration was conducted in August 1999 at a live test range, the L Range at the Army Research Laboratory's (ARL) Blossom Point Facility. Towed-array magnetometer (one pass) and EM pulsed-induction data (two orthogonal passes) over the 3 acre site were collected in 12 survey hours. After analysis of the resulting data sets, 201 targets were classified by their EM response coefficients and flagged for remediation. Target remediation and identification required 12 man-days.

Of the 188 targets recovered from this test area, 66 were ordnance items, 20 were ordnance-related items, 66 were exploded fragments, and 36 were items not related to ordnance. The ordnance items broke down into three groups: 48 81-mm mortars, 8 mortars of smaller sizes, and 10 miscellaneous ordnance items.

The results of our analysis are presented graphically and receiver operating characteristic (ROC) curves are derived and compared to the baseline MTADS magnetometer analysis. For a single ordnance item, 81-mm mortars, we achieve roughly a 60% reduction in false alarms without impacting probability of detection (PD). In order to identify the small fuzes in this field as ordnance, a large number of clutter items have to be included as we are able to reject only ~25%. In part, this is the inevitable result of trying to discriminate ordnance ranging in size from fuzes to 5-in rockets from clutter. This difficulty may be mitigated by obtaining more data, hence better fit statistics, on the smaller ordnance items.

The second demonstration was conducted in September 2001 at the Impact Area of the Badlands Bombing Range, South Dakota site that has been used as an artillery training area for many years. The demonstration was conducted on a portion of the site that had been cleared of ordnance in a previous MTADS demonstration. Twenty-five inert projectiles were seeded on the test area amid the existing clutter field. This was considered a good test of the discrimination

ability of the new analysis algorithms. Magnetometer and EM61 Mk I (single time gate as used in the first demonstration) and EM61 Mk II (four time gates) data were collected.

The EM61 MkII (a relatively new sensor from Geonics, Limited) data proved to be of too low signal-to-noise ratio to be useful in classification. Using the EM61 MkI data, 70 anomalies exhibited signal amplitudes of at least twice the (relatively high) background. Several classification methodologies were employed on these anomalies, and the results are presented graphically.

Compared to a traditional mag-and-flag survey, these methods cost 25% more per acre. Considering that mag-and-flag surveys detect only ~35% of deeper targets, these methods are far more cost effective on a detected target basis. The false alarm rejection mentioned above is not applicable to a mag-and-flag survey.

2.0 TECHNOLOGY DESCRIPTION

2.1 BACKGROUND AND INTENDED USE

Buried UXO is one of the Department of Defense's (DoD) most pressing environmental problems. Not limited to active ranges and bases, UXO contamination is also present at DoD sites that are dormant and in areas adjacent to military ranges that are under the control of other government agencies and the private sector.

Traditional methods for buried UXO detection, characterization, and remediation are labor-intensive, slow, and inefficient. Typical detection and characterization methods rely on hand-held detectors operated by explosive ordnance disposal (EOD) technicians who walk slowly across the survey area. This process has been documented as inefficient and marginally effective.¹ A large portion, approaching 70% in some cases, of the total budget of a typical remediation effort is spent on digging targets that do not turn out to be UXO.

ESTCP has supported NRL in developing MTADS to address these deficiencies. MTADS incorporates both cesium vapor full-field magnetometers and EM pulsed-induction sensors in linear arrays that are towed over survey sites by an all-terrain vehicle. Sensor positioning is provided by state-of-the-art real-time kinematic (RTK) global positioning system (GPS) receivers. The survey data acquired by MTADS is analyzed by an NRL-developed data analysis system (DAS). DAS was designed to locate, identify, and categorize all military ordnance at its maximum self-burial depth. It is efficient and simple to operate by relatively untrained personnel.

The performance of the MTADS has been demonstrated at many prepared sites and live ranges for the past 2 years.²⁻¹¹ It can detect and locate ordnance with accuracies on the order of 15 cm.⁵ However, even with careful mission planning and preliminary training, there are still significant numbers of nonordnance targets selected. Thus, more effective discrimination algorithms are required.

This program was organized on the premise that classification based on shape is central to the problem of discriminating between UXO and clutter. Most UXO fit a specific profile: they are long and slender with typical length-to-diameter aspect ratios of four or five. Many clutter items, on the other hand, do not fit this profile. Using pulsed-induction sensor data, we have developed a model-based estimation procedure to determine whether or not a target is likely to be a UXO item. The model relies on exploiting the dependence of the induced field on target size, shape, and orientation.

2.2 TECHNOLOGY DESCRIPTION

The standard MTADS technology has been described in detail previously.¹² Briefly, the system hardware consists of a low-magnetic-signature vehicle that is used to tow linear arrays of magnetometer and pulsed-induction sensors to conduct surveys of large areas to detect buried UXO. The MTADS tow vehicle, manufactured by Chenoweth Racing Vehicles, is a custom-built off-road vehicle, specifically modified to have an extremely low magnetic signature. Most

ferrous components have been removed from the body, drive train, and engine and replaced with non-ferrous alloys.

The MTADS magnetometers are Cs-vapor full-field magnetometers (Geometrics Model 822ROV). An array of eight sensors is deployed as a magnetometer array. The time-variation of the Earth's field is measured by a ninth sensor deployed at a static site removed from the survey area. These data are used to correct the survey magnetic readings. The pulsed-induction sensors (specially modified Geonics EM61s) are deployed as an overlapping array of three sensors. The sensors employed by MTADS have been modified to make them more compatible with vehicular speeds and to increase their sensitivity to small objects.

The sensor positions are measured in real-time (5 Hz) using the latest RTK GPS technology. All navigation and sensor data are time-stamped and recorded by the data acquisition computer in the tow vehicle. The DAS contains routines to convert these sensor and position data streams into anomaly maps for analysis.

The standard MTADS analysis method has also been described previously.¹³ The magnetometry data has been very successfully modeled using a dipole response. We routinely recover target x,y positions to within 15 cm and target depths to $\pm 20\%$.⁵ Within the signal-to-noise ratio of the MTADS, we see no residual signature attributable to higher moments.¹³ The pulsed-induction modeling has been less successful. The standard algorithm is based on a sphere model and does not represent well the signatures we obtain. We have discussed the deficiencies of this model and proposed an ordnance model based on a prolate spheroid.¹³

This program was organized on the premise that classification based on shape is central to the problem of discriminating between UXO and clutter. Most UXO fit a specific profile: they are long and slender with typical length-to-diameter aspect ratios of four or five. Many clutter items, on the other hand, do not fit this profile. Using pulsed-induction sensor data, we have developed a model-based estimation procedure to determine if a target is likely to be a UXO item. The model relies on exploiting the dependence of the induced field on target size, shape, and orientation.

The EM61 is a time domain instrument. It operates by transmitting a magnetic pulse that induces currents in any nearby conducting objects. These currents produce secondary magnetic fields that are measured by the sensor after the transmitter pulse has ended. The sensor response is the voltage induced in the receiver coil by these secondary fields and is proportional to the time rate of change of the magnetic flux through the coil. The sensor integrates this induced voltage over a fixed time gate and averages over a number of pulses. An illustration of the magnitude and direction of the field transmitted by the MTADS array is shown in Figure 1. Note that the field experienced by an object directly below the array is substantially different from an object in front of or behind the array. This difference allows us to get several "looks" at the target as we conduct a survey, and it aids greatly in our model fits.

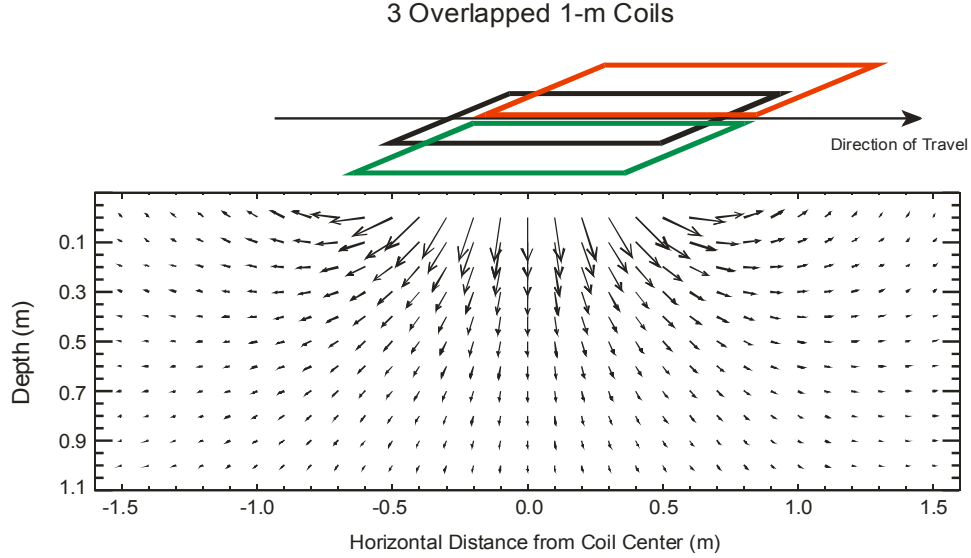


Figure 1. Direction and Magnitude of the Magnetic Field Transmitted by the MTADS EM61 Array.

The model used in these demonstrations has been jointly developed by NRL and AETC Incorporated and has been described recently.^{14,15} Briefly, it relies on the fact that the EM61 signal is a linear function of the flux through the receiving coil. The flux is assumed to originate from an induced dipole moment at the target location given by:

$$\mathbf{m} = \mathbf{UBU}^T \cdot \mathbf{H}_0$$

where \mathbf{H}_0 is the peak primary field at the target, \mathbf{U} is the transformation matrix between the coordinate directions and the principal axes of the target, and \mathbf{B} is an empirically-determined, effective magnetic polarizability matrix. For any arbitrary compact object, this matrix can be diagonalized about three primary body axes and written as:

$$\mathbf{B} = \begin{bmatrix} \beta_x & 0 & 0 \\ 0 & \beta_y & 0 \\ 0 & 0 & \beta_z \end{bmatrix}$$

The relative magnitudes of these β s are determined by the size, shape, and composition of the object as well as by the transmit pulse and fixed time gate of the EM61. Different time gates may result in different values and different relative values of these β s for a given object. The transformation matrix contains the angular information about the orientation of these body axes.

For an axisymmetric object, \mathbf{B} has only two unique coefficients, corresponding to the longitudinal (β_l) and transverse (β_t) directions:

$$\mathbf{B} = \begin{bmatrix} \beta_l & 0 & 0 \\ 0 & \beta_t & 0 \\ 0 & 0 & \beta_t \end{bmatrix}$$

Empirically, we observe that for elongated ferrous objects such as cylinders and most UXO, the longitudinal coefficient is greater than the transverse coefficient. For flat ferrous objects such as disks and plates, the opposite is true. This matches the behavior of these objects in the magnetostatic limit. For nonferrous objects such as aluminum cylinders and plates, these relationships are reversed.

We tested several implementations of this model in our early shakedown demonstrations. All were designed to take advantage of the fact that we obtain reliable position (x,y,z) information from the magnetometer signals. We then fitted the pulsed-induction response to models with combinations of two or three response coefficients, β , and two or three orientation angles. One goal of these shakedown demonstrations was to determine which of these models resulted in the most classification utility with the least data collection expense. We have determined that conducting two orthogonal EM surveys and fitting the data using the three β , three angle model yields the optimum results. This survey methodology, discussed below, was used in these demonstrations.

2.2.1 Mobilization and Operational Requirements

All MTADS equipment is designed to be transported to field sites to support survey and remediation operations. All electronic instrumentation and office equipment is equipped with foam-padded containers that can be shipped by air or truck. All field equipment is designed to be transported by a tractor-trailer. We pack and transport an extensive list of spare equipment and components for field repair and replacement. Small electronics and mechanical repair stations are packed and resupplied before each deployment. We have dedicated communications and two-way radio equipment to support the field operations. Battery charging stations are carried to support all radios, electronics, and navigation equipment.

We mobilize to survey sites using a rented tractor-trailer. This rental is economical enough that the rig is typically left on site throughout the survey for storage of spares. All MTADS equipment required for a mag and EM survey can be accommodated in a 53-ft trailer. At some sites, electrical power, water, and office facilities are available to support our operations. More typically, one or several of these are not available on site and are leased and delivered to the site before MTADS operations begin. Typical logistics support requirements and their rental costs are shown in Table 1.

Table 1. Typical Logistics Costs for a 2-Week Survey Assuming No Remediation.

Activity	Cost (\$K)	Total (\$K)
Presurvey Expenses		
Initial site visit	3.0	
Establish navigation control points	12.0	
Draft demonstration plan, health, and safety work plan	15.0	
Presurvey total		30.0
Equipment Transport		
Truck rental	3.5	
Fuel, permits, and tolls	1.0	
Driver	1.5	
Subtotal for equipment transport		6.0
On-Site Logistics		
Office trailer	3.0	
Electrical hookup	1.0	
Portable toilets	1.0	
Power generator and fuel	3.5	
Tent for equipment repair	1.5	
Subtotal for on site logistics		10.0
TOTAL		46.0

2.2.2 Personnel and Training Requirements

MTADS surveys to date have been overseen by a senior research scientist. Although, in the strictest sense, this results in an over-qualified field supervisor, we find it to be an efficient deployment of resources. Small problems are avoided or solved more quickly and our total productivity is higher with a senior supervisor. In a commercial environment, where survey jobs are more frequent and of longer duration, this senior supervisor may be required on site only for the first few days of the survey, then, available for telephone consultation.

The field operations and data collection are carried out by a single vehicle operator who doubles as the site safety officer. Because of this dual role, we employ a retired EOD technician for this position. If a site has a separate safety officer, the requirements for vehicle operator would be a standard geophysical field technician. Survey guidance, reorienting the driver after turns, and general maintenance and housekeeping are provided by three to five laborers from the local labor pool. On most sites, these laborers are required to be hazardous waste operations (HAZWOPR) certified.

MTADS demonstration surveys have all been carried out with simultaneous or overlapping remediation operations. This requires the presence of experienced data processing and data analysis personnel on site. If remediation is to be accomplished at a later date, only a BS-level data analyst is required on-site for quality control (QC) purposes. In this case, the trained analyst can work from home base. One of the goals of this project is to make the data analysis more routine so that less-trained employees can be productive. We have made some progress in this direction but have not succeeded completely.

When working on live ranges or former bombing or gunnery targets, we routinely conduct a walkover and surface clean prior to conducting vehicular surveys. The surface walkovers are carried out by subcontractor UXO-certified specialists. The typical team consists of one UXO-certified supervisor and five laborers. Depending on the circumstances, the laborers either have HAZWOPR certification or are trained on site by the UXO supervisor.

2.2.3 Health and Safety Training

Many workers on a survey are required to have HAZWOPR and/or UXO certification, and a health and safety work plan is required on all UXO operations. This work plan contains detailed descriptions of the hazards expected on site, standard procedures for identifying these hazards, protocols for dealing with them, and emergency health care procedures.

2.3 ADVANTAGES AND LIMITATIONS OF THE TECHNOLOGY

We have demonstrated^{5,7} that an impressive level of discrimination is possible using the baseline MTADS if a small training area is investigated prior to data analysis on the entire site and if the distribution of ordnance types is limited. This discrimination is based primarily on fitted dipole size. In this program we have demonstrated methods designed to add shape as an extra dimension to the discrimination. For items with similar induced magnetic dipoles, we can discriminate based on the ratio of responses along the item's three axes to the EM induction sensors in the MTADS suite. As shown in a later section, this adds some discrimination capability to the system.

Even with the most optimistic result, however, these methods will not result in a perfect system. As we have stated above, this program is based on the idea of classification by shape. By definition, this implies that clutter items with shapes similar to ordnance will be classified as ordnance, e.g., pipes and post sections. If it is important to reduce remediation costs to the extent that these items are not dug, other methods, possibly sensitive to composition or the presence of explosive compounds, will have to be employed in conjunction with those developed in this program.

3.0 DEMONSTRATION DESIGN

3.1 PERFORMANCE OBJECTIVES

The objective of these demonstrations was to quantify the classification performance available using commercially available pulsed-induction sensors and the data modeling algorithms developed in this program. The demonstrations proceeded in three phases: data collection, data analysis, and target marking and remediation.

3.1.1 L Range Demonstration

Data collection consisted of surveying an area of approximately 3-acres on a live range, known to have had many detonations, using magnetometers and pulsed-induction sensors. The magnetometer survey was conducted in an E-W orientation to minimize the effects of vehicle self-signature. The pulsed-induction survey was carried out both E-W and N-S to get the best possible illumination of each target.

Data were analyzed using the MTADS data analysis system, modified to include the 3- β approach. This upgrade allows simultaneous analysis of a magnetometer and several pulsed-induction survey data sets. The analysis consists of fitting individual target signatures to the model described above to extract target position, size, and relative response coefficients along three orthogonal axes. We planned to select ~200 targets for remediation. After analysis of the survey data, we found that there were only ~200 targets in the survey area with signatures well enough separated to get a good model fit so no further selection was necessary. This target set represents ~25% of those targets with magnetic anomaly > 50nT and/or EM anomaly > 70mV. In our view, this is a large enough fraction of the total targets to ensure that a representative sample of all targets was remediated. The relative fitted response coefficients were used to classify the target as UXO or scrap. This resulted in a spreadsheet-like target report that included target number, location, depth and predicted class. This spreadsheet and the reasoning behind the target assignments was communicated to personnel from the Institute for Defense Analyses (IDA) before digging the selected targets.

The final phase of the demonstration consisted of flagging and digging the selected targets by a commercial UXO firm. Careful remediation notes were made for each target that included actual target location, field identification of the target, rough target dimensions, and a photograph of each target. These field results, in conjunction with the fitted target responses, provided the basis for quantitative evaluation of this method's classification performance. Later sections of this report will present these results in detail.

3.1.2 BBR Impact Area Demonstration

This demonstration involved three MTADS vehicular surveys—a magnetometer survey of 10 seeded acres east of the previously identified bull's eye on the impact area, an EM61 MkII survey of the same area, and an EM61 MkI survey of the area.

The survey data from the first three surveys were analyzed in the following ways:

- MTADS baseline analysis (only magnetometer data)
- 3- β analysis using each of the EM data sets
- Probabilistic neural net (PNN) analysis (from the NRL Strategic Environmental Research and Development Program [SERDP]) using baseline MTADS magnetometer predictions.

The specific objective of this demonstration was to produce a quantitative comparison among the data analysis methodologies listed above, including probability of detection and false alarm (FA) rate. After initial analysis of the data, we were able to add a comparison of the performance of the EM61 sensor array in low- and high-signal to noise ratio (SNR) environments to this list. We also developed alternative discrimination methods that show more promise under these conditions. These topics are addressed in the following section.

The seed target area is within a few hundred meters of the bull's eye identified in the 1999 survey and therefore has a high concentration of fragments and scrap (primarily pieces of auto parts from the target) on and near the surface. This provides a stringent test for the methods being demonstrated. Section 5 discusses the influence on classification of this high noise field.

3.2 SELECTION OF TEST SITES

The site of the first demonstration, the L Range at the ARL's Blossom Point Facility, was chosen to be a realistic test of the methods developed in this program. The range has been used for a variety of mortar and barrage rockets and contains large amounts of clutter and scrap. The preliminary testing in this program was conducted on a test field with mostly ordnance and ordnance-simulants, which were appropriate for model development but not particularly representative of a live-site situation. This range is a good model site for demonstrating this technology.

In 1999 we conducted a demonstration survey on the impact area (previously referred to as the Air Force retained area) on the Badlands Bombing Range (BBR).¹⁶ In preparation for this work, NRL conducted site visits, records searches, tribal coordination activities and acquired aerial photography and presurveying of first-order control points to support the activity.

This site is ideal for the purposes of the second demonstration. It has been used for years for gunnery practice and is thus covered with fragments ranging from small to large. It has fragment clusters that apparently result from underground explosion of practice projectiles. These fragment clusters have magnetic signatures virtually indistinguishable from that of an intact 105-mm projectile. Thus, if there is value in these analysis methods, it can be demonstrated at this site.

3.3 TEST SITE HISTORY AND CHARACTERISTICS

3.3.1 L Range Demonstration

During World War II, Harry Diamond and his team at the National Bureau of Standards (NBS), now named the National Institute of Standards and Technology (NIST), needed open areas to test fuzes they were developing. They established test sites at Aberdeen Proving Ground, Maryland; Fort Fisher, North Carolina; and, in early 1943, NBS leased land and established a proving ground for proximity fuzes at Blossom Point. By September 1945, 14,000 rocket and mortar rounds had been fired. In 1953, the lease on the property was transferred to the Army, which operated the property as a fast-reaction, low-cost range for experimental work. Firing ranges provided a 2000-yard maximum range for land impact and a 10,000-yard maximum for water impact. During the Vietnam War, the Army's Harry Diamond Laboratory was very active at the site.

The L Range is the main range for impact testing of various munitions at Blossom Point. It is approximately 800 feet wide by 5,000 feet long and encompasses ~93 acres. This range has been the primary impact area throughout the history of the site. Some of the known firings include 81-mm mortars in 1961, 2.75-inch rockets fired from helicopters throughout the 1970s, a variety of experimental 60-mm mortars, 75-mm projectiles, 81-mm mortars, and various barrage rockets.

HFA, Inc. conducted an ordnance removal at the Blossom Point Test Facility in 1996.¹⁷ Two sites totaling 66 acres were cleared in conjunction with utility work and construction, one a clear area parallel to L Range and one a wooded area north of the first. Targets were dug to 4 feet on the construction sites and 2 feet for the utility easements. Seven hundred fifty-three UXO items and 9,267 lbs. of scrap were removed from the site. The UXO included a wide variety of ordnance types and classes with a preponderance of 20- and 30-mm rounds, 60- and 81-mm mortars, and 4.2-in rockets. This is consistent with the firing records.

Figure 2 is a road map of a portion of Charles County, Maryland, showing the location of Blossom Point relative to La Plata, the county seat. The ARL Blossom Point Facility is classified as a range and therefore is closed to the public. Access to DoD employees and contractors is limited by the operating hours of the facility. Figure 3 is an aerial photo of the Blossom Point Field Facility with the final demonstration test site area highlighted in yellow.

The demonstration area is located on high ground, well above the surrounding rivers. The site has good sky view for GPS but is bordered by a densely wooded area that is ideal for testing non-GPS location systems. This demonstration was carried out in the GPS-accessible portion of the site.

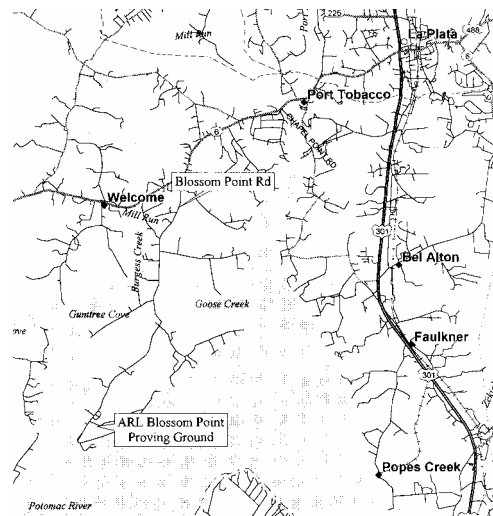


Figure 2. Road Map Showing Location of the L Range.



Figure 3. Aerial View of the Army Research Laboratory Blossom Point L Range with Approximate Location of the First Demonstration Highlighted.

3.3.2 BBR Impact Area Demonstration

In 1942 the Department of War annexed 341,725 acres of the Pine Ridge Reservation for use as an aerial gunnery and bombing range. This site is in the southwest corner of South Dakota, with the largest part of the Bombing Range in Shannon County. From 1942 until 1948, various sections of this range were used for bombing exercises and various air-to-ground operations. Since 1960, portions of the land have been returned to the Oglala Sioux Tribe (OST) in a step-wise fashion. In 1968, Congress enacted Public Law 90-468, returning 202,357 acres to the OST and setting aside 136,882 acres of formerly held tribal lands to form the Badlands National Monument, to be managed by the National Park Service. In 1978, all remaining BBR lands were declared excess with the exception of 2,486 acres, referred to as the impact area. Around 1965, the South Dakota National Guard placed up to 100 car bodies on the 2,486-acre area and began using them as artillery targets during training exercises. The National Guard training exercises took place on the impact area between 1966 and 1973.

Figure 4 is a portion of a U.S. Geological Survey (USGS) 7.5-minute topographic map showing the location of the retained area outlined in red. The retained area range is surrounded by a buffer zone generally of about 1,000 meters. The retained area perimeter fence is shown in red, portions of the buffer boundary in green. A second perimeter fence is located at the outer border of the buffer zone. The most direct access to the retained area is by a dirt road that exits to the south from Highway 40. The dirt road was graded, including installation of some culverts, to support the 1997 Air Force EOD clearance activities. There is only one fence internal to the retained area.

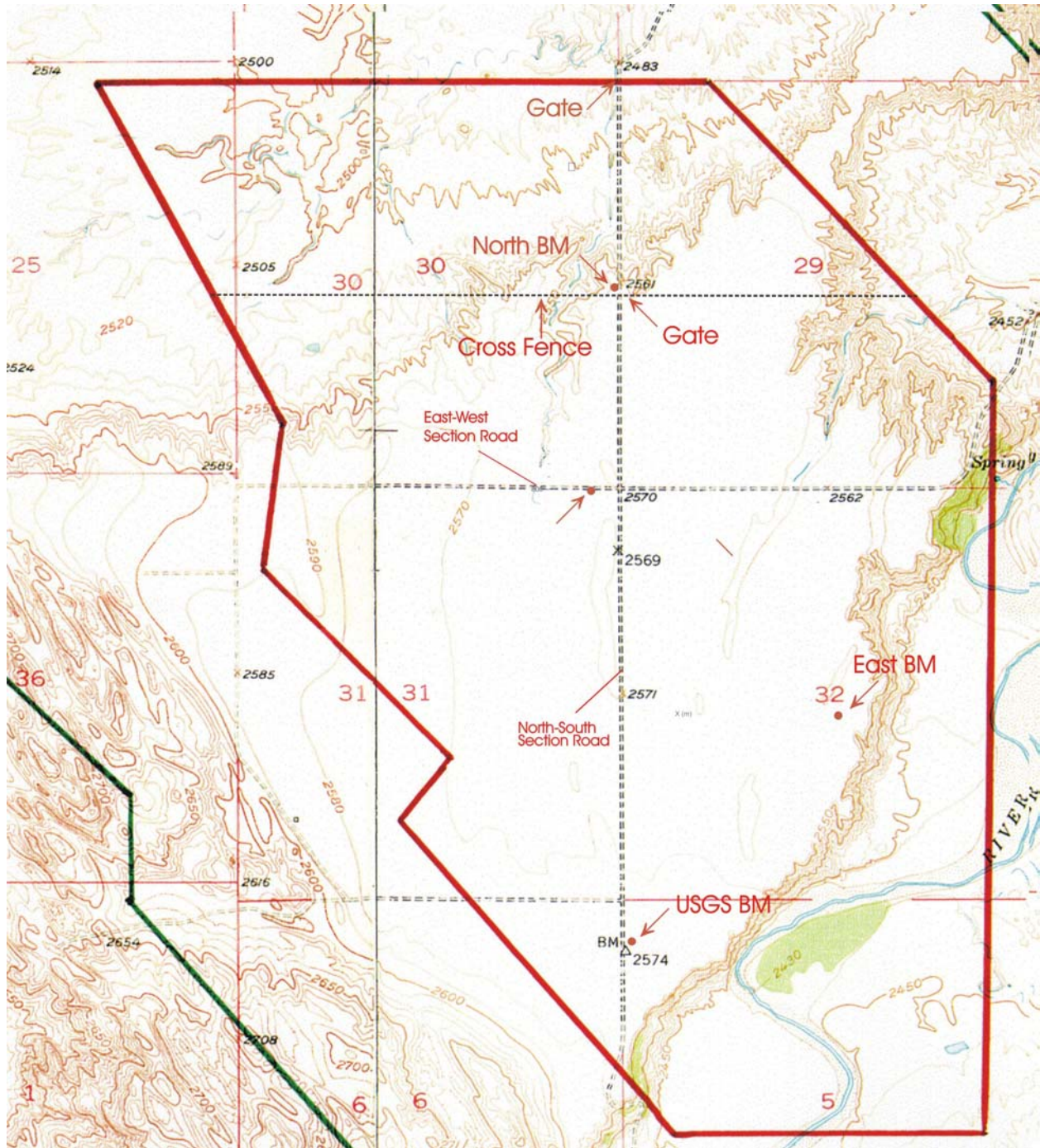


Figure 4. A Portion of a USGS 7.5-Minute Map with the Perimeter of the BBR Impact Area Shown in Red. (Relevant roads, fences, and survey control points are also shown.)

This east-west fence bisects sections 29 and 30 and is labeled “cross fence” in Figure 4. Three geodetic survey points are located on the retained area. These sites, labeled North BM, East BM, and USGS BM were upgraded to “near first-order” by Ellsworth Air Force Base (AFB) Civil Engineer Squadron (CES) personnel using the OST 5 benchmark. The latter point was established by NRL contractors in 1997 and is legitimately first order. All 1999 NRL surveys were done using the North BM coordinates provided by Ellsworth AFB. The coordinates of these points are given in Table 2.

Table 2. Impact Area Survey Coordinates Provided by Ellsworth AFB.

Point	Latitude	Longitude	Northing (m)	Easting (m)	Height (m)
			NAD 83		
OST 5	43° 42' 05.2702”	-102° 18' 35.5186”	4842233.05	716761.31	804.460
North BM	43° 40' 19.1197”	-102° 14' 20.5113”	4839145.82	722578.26	762.530
East BM	43° 39' 21.2053”	-102° 13' 42.8268”	4837387.2	723481.89	764.260
USGS BM	43° 38' 53.7820”	-102° 14' 18.7564”	4836514.29	722705.23	765.940

3.4 PHYSICAL SETUP AND OPERATION

3.4.1 L Range Demonstration

Since this demonstration was conducted on the Blossom Point site adjacent to where our equipment is housed, many of the normal presurvey logistics listed in Table 1 such as establishing first-order GPS markers, transporting equipment to the site, and setting up and testing equipment were not required. We performed the demonstration “out of the garage.” In all other ways, this demonstration was conducted in accordance with our normal survey practices. The actual demonstration schedule is shown in Table 3.

Table 3. Schedule for the L Range Demonstration.

Date	Activity	Required Time
29 July 1999	Magnetometer survey of site	2 hrs survey time
3 August 1999	East-west EM survey of site	5 hrs survey time
	North-south EM survey of a portion of the site	1 hr survey time
4 August 1999	North-south EM survey of remaining area	4 hrs survey time
	Data analysis and target classification	
12-13 August 1999	Flag targets for remediation	16 man-hours
16-18 August 1999	Target remediation	12 man-days
26 August 1999	Required demolition—81 shots on 73 targets	

3.4.2 BBR Impact Area Demonstration

Inert ordnance from the Aberdeen Test Center (ATC) at Aberdeen Proving Ground (APG), Maryland was used to establish the seed area. ATC degaussed the ordnance and transferred it to the Engineer Research and Development Center (ERDC) in Vicksburg, Mississippi for emplacement on the site. Mr. Tommy Berry of ERDC emplaced the inert targets on the site in August 2001. The seed area corners were provided to ERDC by NRL. The targets were

emplaced using a slanted auger so there would be no visible surface scars above the ordnance. The ground truth for the seeded targets was held by ERDC until after the completion of the survey. It was not available to any individual data analyst until the completion of their assigned analyses. Table 4 lists a seed target locations and orientations.

Table 4. Location of Emplaced Seed Targets at the Impact Area.

Item #	Northing (m)	Easting (m)	Depth (m)	UXO Type	Azimuth (°)	Incline (°)	Nose U/D	Serial Number
1-2	4,838,171.34	722,824.74	0.75	8-inch	350	75	D	4
1-4	4,838,142.67	722,957.56	0.50	8-inch	270	45	D	5
1-6	4,838,117.82	722,874.46	0.75	8-inch	40	80	D	3
1-8	4,838,082.55	722,834.30	0.30	8-inch	10	0	H	6
1-10	4,838,019.39	722,889.76	0.50	8-inch	340	40	D	2
1-12	4,838,120.88	722,786.50	0.85	155-mm	0	45	D	10
1-14	4,838,086.48	722,802.76	0.25	155-mm	250	65	D	8
1-16	4,838,176.31	722,813.27	0.60	155-mm	15	80	D	12
1-18	4,838,143.69	722,819.03	0.85	155-mm	115	45	D	11
1-20	4,838,066.32	722,848.56	0.25	155-mm	165	70	D	13
1-22	4,838,142.69	722,860.13	0.25	155-mm	110	0	H	15
1-24	4,838,168.67	722,886.90	0.30	155-mm	360	35	D	9
1-26	4,838,106.46	722,901.24	0.55	155-mm	75	45	U	14
1-28	4,838,202.03	722,921.32	0.60	155-mm	30	40	D	6
1-30	4,838,137.07	722,919.42	0.40	155-mm	310	55	D	7
1-32	4,838,196.19	722,853.42	0.25	105-mm	110	35	D	16
1-34	4,838,176.23	722,831.42	0.92	105-mm	5	75	D	9
1-36	4,838,174.21	722,879.23	0.40	105-mm	115	45	D	10
1-38	4,838,164.65	722,931.82	0.25	105-mm	30	0	H	7
1-40	4,838,141.72	722,893.58	0.50	105-mm	50	55	D	13
1-42	4,838,118.78	722,830.47	0.60	105-mm	245	75	U	15
1-44	4,838,070.04	722,926.09	0.50	105-mm	65	60	D	12
1-46	4,838,064.41	722,957.64	0.25	105-mm	315	80	D	11
1-48	4,838,050.93	722,914.61	0.30	105-mm	25	35	D	8
1-50	4,838,032.77	722,808.48	0.30	105-mm	360	45	D	14
Corners								
NW	4,838,214.74	722,778.78						
NE	4,838,214.73	722,978.77						
SE	4,838,014.77	722,978.76						
SW	4,838,014.73	722,778.79						

No logistics support was available on the BBR site so all support equipment had to be rented in Rapid City, South Dakota, and trucked 75 miles to the impact area site. Figure 5 is an aerial photo of the MTADS base camp set up just south of the cross fence shown in Figure 4 and east of the Section Road. One of the office trailers served as a data analysis and electronics repair office; the next was used for equipment storage and battery charging; the next supported the tribal workers and



Figure 5. Aerial Photograph of Logistics Support for the Second Demonstration.

remediation contractors; and the final, a drive-through trailer, housed the vehicular MTADS tow vehicle and trailers. Also shown in the photo is a tent set up to provide cover from the elements during work breaks and repair and maintenance of the vehicle and sensor trailers and the tractor-trailer used to transport equipment to the site from our base in Blossom Point, MD. The tank truck at the southern end of the camp was used to support the concurrent airborne MTADS survey of the site. Finally, the diesel generator and portable toilets are shown to the east of the office trailers.

The demonstration schedule is detailed in Table 5. There were several delays associated with equipment breakdowns that were exacerbated by the airline and shipping delays associated with the events of September 11, 2001. Ultimately, these delays had no significant impact on the demonstration.

Table 5. Schedule for the BBR Impact Area Demonstration.

Date	Activity	Comment
6 September 2001	MTADS equipment arrives on site	
7 September 2001	Equipment unpacked and assembled	
9 September 2001	Survey personnel arrive on site	
10 September 2001	Begin EM61 MkII calibration	Hardware failure; electronics shipped to Canada for repair
11 September 2001	Begin magnetometer survey of seed area	
12 September 2001	Complete seed area survey, begin airborne support areas	
15 September 2001	Complete vehicular magnetometer surveys	
17 September 2001	Begin EM61 MkI calibration	Center sensor fails; return to Canada for repairs
18 September 2001	EM61 MkI survey of seed area without center sensor	EM61 MkII returns
19 September 2001	Reinstall EM61 MkII following repairs	
20 September 2001	EM61 MkII N/S survey of seed area	
21 September 2001	EM61 MkII E/W survey of seed area	EM61 MkI returns
22 September 2001	EM61 MkI E/W survey of seed area	
23 September 2001	EM61 MkI N/S survey of seed area	
1 October 2001	Dig teams waypoint seed area	
23 November 2001	Remediation complete	

4.0 PERFORMANCE ASSESSMENT

4.1 L RANGE DEMONSTRATION

4.1.1 Remediation Results

After completion of the magnetometer and two EM surveys in perpendicular directions, 201 targets were analyzed and marked for remediation on the L Range Final demonstration site. A total of 188 targets were recovered from this test area, 13 of which were dry holes. Examples are pictured in Figure 6 and Figure 7. There were 66 ordnance items, 20 ordnance-related items (rocket motors with fins and mortar tail booms), 66 exploded fragments, and 36 items not related to ordnance. The ordnance items broke down into three groups: 48 81-mm mortars, 8 mortars of smaller sizes, and 10 miscellaneous ordnance items. The miscellaneous items included 2 bomb fuzes, a 76-mm projectile, and two 5-in rockets. The exploded fragments appeared to be mostly from mortar casings. The nonordnance items included cable tie down points for test towers that had been removed, block and tackles from the cables, and a variety of odd scraps of metal (rebar, sheet metal, angle iron, and bolts).



Figure 6. Example 81-mm Mortar (left panel) and 60-mm Mortar (right panel) Remediated at the L Range.



Figure 7. Example of Nonordnance Remediated at L Range. (This item is part of a block and tackle used for guy-cables for a test tower.)

An abbreviated version of the MTADS target report for these items is attached as Appendix B. Included in this report are the results of the magnetometer and 3β analyses and the field notes on the identity of the remediated items. As the goal of this demonstration was to validate the

utility of the 3β analysis for target classification, all remaining discussion focuses on that analysis.

4.1.2 Performance Data

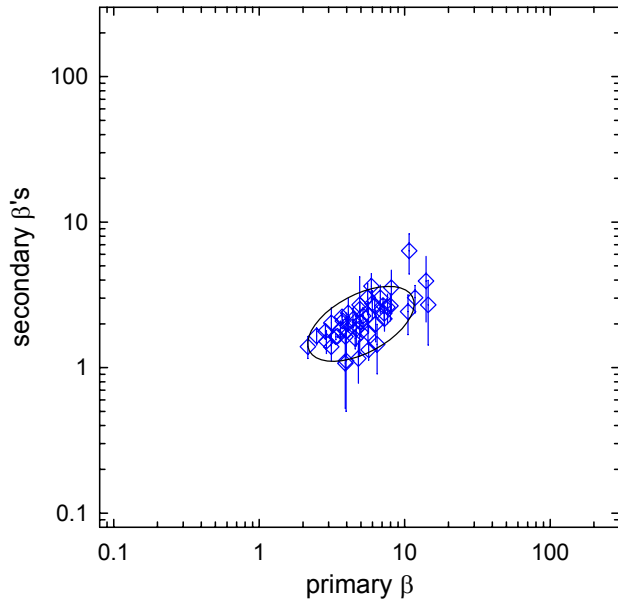


Figure 8. Two-Dimensional Representation of the Three-Beta Fits for the 81-mm Mortars in the Demonstration.

We will concentrate our initial discussion on the 81-mm mortars as they provide the best fit statistics. The results of the three-beta fits for the 81-mm mortars are shown in Figure 8. The value of the primary beta (largest) is plotted on the abscissa. The two smaller betas are plotted on the ordinate, where the symbol in the plot is the average and the vertical line represents the spread between the two values. We find this to be an easier way to visualize the spread in the data than plotting the points in three dimensions. Note that if the fit results were perfect (no measurement errors), the data would all be symbols with no vertical line (secondary betas are equal for axisymmetric objects). In the Final Report¹⁸ for this program we detailed results from bench tests that confirm this.

The three beta values for the 81-mm mortars are best described by a log-normal distribution. In logarithmic quantities, the mean is 0.697, 0.318, and 0.310 with standard deviations of 0.2, 0.09, and 0.13 for β_1 , β_2 , and β_3 respectively. In measured units, this corresponds to an average response of 4.98 along the length of the mortar and 2.0 transverse to this. Note that the values range from 2 to 12 along the primary axis, which is much greater than the 20-30% observed in preliminary testing for objects in our test field. It is thought that this enlarged spread is largely due to positioning errors in height, as the array is towed over the uneven ground of a live site. We will discuss this point in more detail later in the report. The ellipse plotted in Figure 6 represents a three-dimensional ellipsoid with major and minor radii that are equal to two standard deviations of the primary and secondary betas. The ellipse is tilted because of a weak correlation between the primary versus the secondary betas (stronger primary betas correlate with stronger secondary betas). As explained below, this ellipsoidal curve can be used to calculate the probability that a given beta fit represents an 81-mm mortar.

The three-beta fit results for the other ordnance items recovered at the L Range are plotted in the left panel of Figure 9. The approximate primary versus secondary beta values range from 0.7/0.5 for the bomb fuze to 178.0/62.0 for the 5-in rockets. A similar plot for the fragments, the ordnance-related scrap, and the nonordnance scrap is presented in the right panel of Figure 9. It is interesting to note that the bulk of the fragments do not overlap the 81-mm mortars. One would expect that a large spread in the secondary betas should result from an

irregularly shaped object. Overall, the spread observed in the right panel of Figure 9 is not much greater than the spread for the axisymmetric ordnance objects (Figure 8 and left panel of Figure 9). After examining photos of the objects dug, this is not too surprising. Most of the scrap, to first order, is elongated, with approximately equal secondary dimensions.

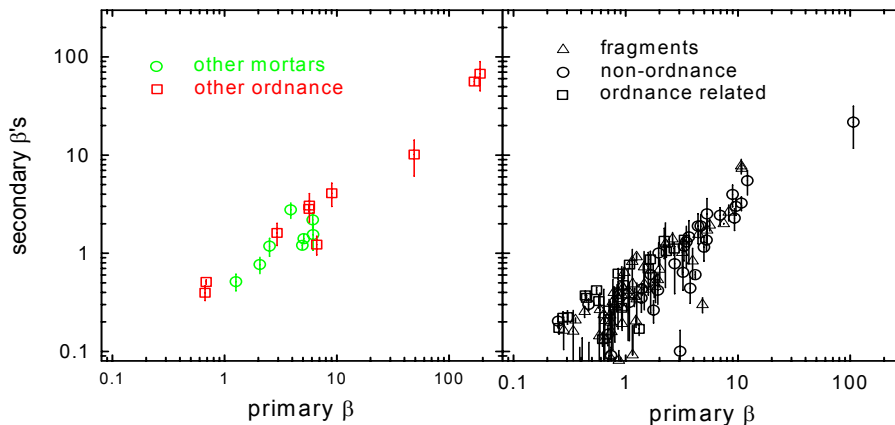


Figure 9. Two-Dimensional Representation of the Three-Beta Fits for Other Targets from the Demonstration Plotted as in Figure 8.

Examples of ROC curves based on the L Range data are shown in Figure 10 and Figure 11. To generate these curves, the ellipsoid in Figure 8 is expanded (in three dimensions) and the number of ordnance PD and non-ordnance false alarm beta values that fall within this three dimensional region are counted. Figure 10 plots the results for a single 81-mm ellipsoid. In Figure 11, ellipsoids are generated about each of the ordnance items present. The sizes of these ellipsoids are expanded uniformly based on the standard deviations and correlations of the 81-mm betas; too few of these other ordnance items were fitted to generate valid beta statistics. This is illustrated on the familiar beta plot in Figure 12.

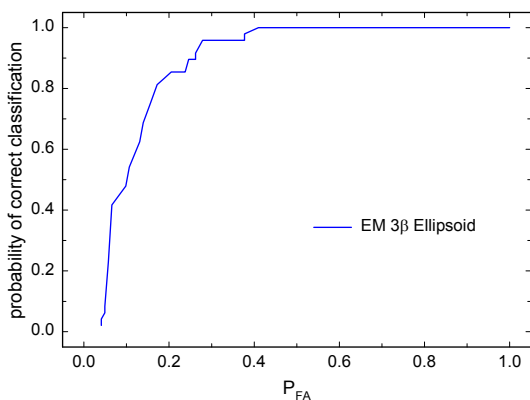


Figure 10. ROC Curve for Detection of 81-mm Mortars.

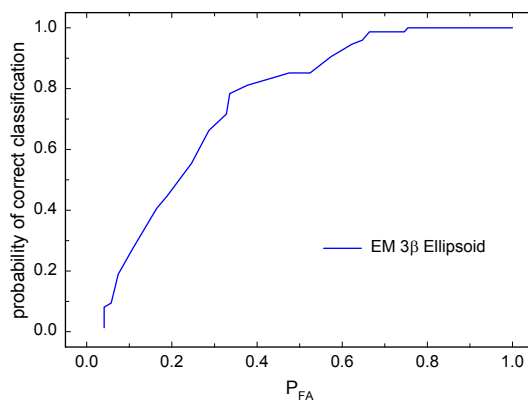


Figure 11. ROC Curve for Detection of All Ordnance.

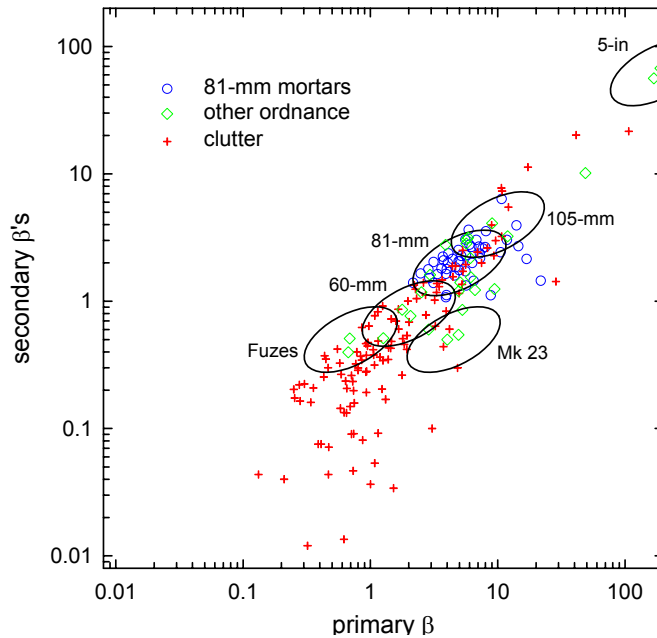


Figure 12. Two-Dimensional Representation of the Three-Beta Fits to All Targets Dug in the Demonstration with Ellipses for Each Ordnance Class Derived from the 81-mm Mortar Ellipse.

The discrimination performance we achieve for a single ordnance item, 81-mm mortars, matches results we have obtained in earlier, controlled tests of this method. We achieve a roughly 60% reduction in false alarms without impacting PD. The story is more complicated when trying to discriminate several classes of ordnance from the background clutter (see Figure 11). We still reduce false alarms by 25%, but in order to identify the small fuzes in this field as ordnance, a large number of clutter items have to be included. In part, this is the inevitable result of trying to discriminate ordnance ranging in size from fuzes to 5-in rockets from clutter. This difficulty may be mitigated by obtaining more data, hence better fit statistics, on the smaller ordnance items. Using the error ellipsoid derived from the distribution of 81-mm mortar fits, as we were forced to do, may well overstate the region of the 3-D space occupied by the smaller ordnance items. As we obtain more model fits to remediated ordnance and improve our fit statistics, we will be able to test this premise.

4.1.3 Data Assessment

The survey data collected during the first demonstration were of sufficient quality to meet the stated goals. We were able to increase the discrimination available using MTADS EM induction survey data for targets with isolated signatures. Several features of the data limited the classification ability, however. We showed in the earlier controlled tests that sensor noise and sensor location error limited the estimated betas to a precision of ~25%. Some improvement is possible in this regard, but not a lot. The GPS units used for sensor location on the MTADS array are state-of-the-art receivers with cm-level precision. Because of the response of the EM61 sensors to the GPS antenna, the antenna is located ~1.5 m in front of the sensor array. Although the antenna location is known to centimeters, there is some location uncertainty introduced by the back projection of the sensor locations from the antenna position.

A two- or three-antenna array, with GPS antennas in front of and behind the EM sensors, would reduce sensor location uncertainties. At the time of this demonstration, this would have involved the purchase of another independent GPS receiver/radio combination. Now, because of the demand from the mining and construction markets, multiple receiver systems are available for a modest increase in price. Such a system was used at the second demonstration at the BBR impact area. Sensor noise is a different issue. Progress here requires a new generation of EM induction sensors.

Compared to the data collected during our initial, controlled tests, there was a decrease in the precision of the fitted beta values during this demonstration. We attribute this to vertical motion of the EM array over the rough ground at the live site. In an attempt to provide some quantitative underpinning to this assertion, we have performed a Monte Carlo simulation of the fitted response of an 81-mm mortar simulant with varying sources of noise. The object used in the simulation had betas of 5,2,2, about that expected for an 81-mm mortar. The object was placed at a distance of 0.6 m from the sensor array and given a random x,y position relative to the survey tracks and a random orientation. Each simulation included real MTADS GPS and sensor noise. The results of this simulation are shown in Figure 13. The top panel shows the results using only GPS and sensor noise. In this case, the fitted betas exhibit just the precision observed in controlled tests, ~25%. For the simulation depicted in the bottom panel of Figure 11, a component of sensor height variation was added to simulate array bouncing over rough ground. We find that red noise with an root mean square (RMS) amplitude of 3 cm reproduces the spread in betas observed in the demonstration. This is easily within the realm of possibility; the MTADS EM array platform does not have a suspension and is observed to bounce in rough terrain.

The terrain at the L Range demonstration was not especially rough for a live-site demonstration—MTADS has been demonstrated at several sites with much more challenging terrain. Therefore, to take advantage of the shape information inherent in the response of targets to the EM61 array, better control of vertical sensor displacements will be required. One option is to add suspension to the array platform. Another possibly more effective method would be to record the displacements of the array using inertial sensors and explicitly account for the position of the array in three dimensions in the data analysis procedure.

4.1.4 Technology Comparison

The obvious baseline for comparison of the value of the technology demonstrated here is the current MTADS. As mentioned above, the baseline MTADS is able to achieve a reasonable level of discrimination using magnetometry fits alone, especially when the ordnance distribution is limited. We will compare the results obtained in this demonstration with those that would be obtained by MTADS at the same site so we have made use of the fitted magnetometer “size” parameter that is included in the target report in Appendix B. For each ordnance class, we calculate a mean size. Just as in the case of the 3-beta algorithm, we are able to calculate a distribution about this mean for the 81-mm mortars. We use the 81-mm size distribution to generate a proportionally-sized distribution for each ordnance class. The distributions derived are listed in Table 6.

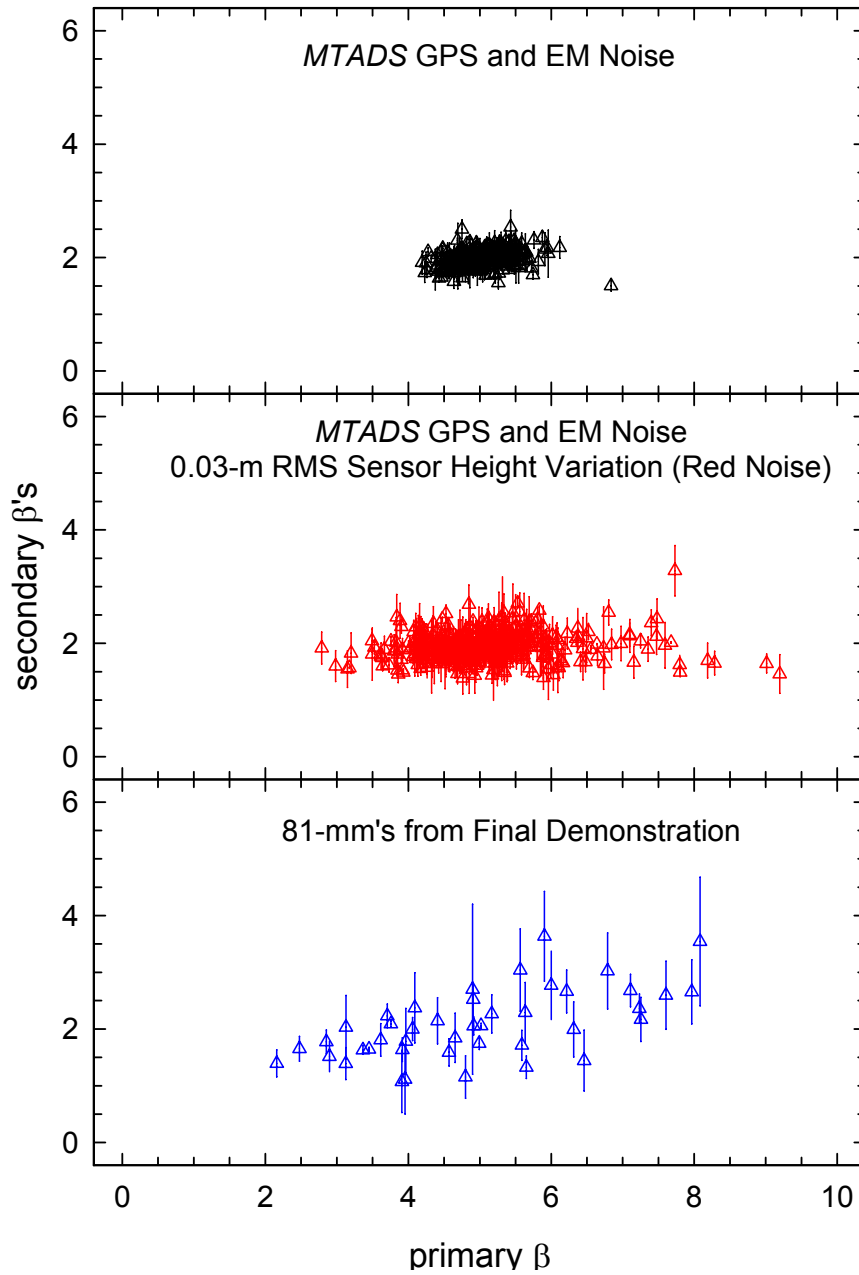


Figure 13. Results of a Monte Carlo Simulation of Fitted Betas Resulting from a Range of Model 81-mm Mortars with Two Sources of Noise Compared to the Results from the First Demonstration.

Table 6. Size Distributions Used in Magnetometer Analysis of the Demonstration Results.

Ordnance Class	Size Distribution (mm)	Ordnance Class	Size Distribution (mm)
Fuzes	43 ± 9	81-mm mortar	76 ± 16
Mk23	56 ± 11	105-mm projectile	105 ± 21
60-mm mortar	60 ± 12	5" rocket	212 ± 42

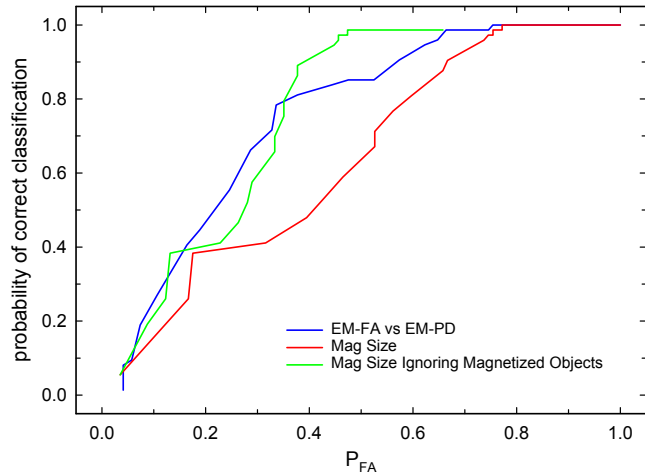


Figure 14. ROC Curve for Classification Using These Methods Compared to Results Using Magnetic Dipole Size and Dipole Orientation.

ordnance recovered at the L Range; only one of the 73 items considered had a magnetic dipole orientation not consistent with an induced dipole only. Note that this method does not automatically eliminate all items with a remanent moment, only those whose net dipole orientation is outside that expected from an item with a wholly induced dipole.

The magnetic dipole size suffers from many of the same problems as the 3-beta algorithm when attempting to discriminate all ordnance. In order to capture the fuzes, many small frag items must be included. The magnetic dipole orientation filter helps greatly in this regard as a good number of the frag items are magnetized and are thus correctly identified as clutter.

It is difficult to compare the performance of the analysis of EM61 data presented here with that of other sensors and analysis methods. As we have shown, the current procedure gives excellent results in the test jig and reasonable results at our Test Field, which is a smooth, clean, and level site. The only legitimate comparison is to results obtained by competing technologies on live-site surveys. As these data become available, direct comparisons will follow.

4.2 BBR IMPACT AREA SURVEY

4.2.1 Pre-Demonstration Measurements

As this demonstration was being planned, the manufacturer of the EM61, Geonics Limited, announced a new version of the sensor, designated the EM61 MkII. This new sensor has the ability to sample the decay of the induced magnetic fields with four independent gates compared to the two gates (one each on the upper and lower receive coils) in the EM61 MkI. This new product opens the possibility of gaining extra discrimination information by sampling a portion of the time-history of the object response coefficients, β . We incorporated this new instrument into the demonstration to test the utility of these new sampling gates.

We can then generate a ROC curve for this method by varying the width of the distribution around each ordnance class and declaring each target as ordnance (within the six size bands) or clutter. The result of this analysis is plotted in Figure 14. Also plotted in Figure 14 is a curve generated by enhancing the magnetometry analysis by taking advantage of the fitted magnetic dipole orientation for each target. This enhancement relies on the observation that UXO targets have, in general, been shock demagnetized by their impact with the ground and only exhibit induced magnetic moments while fragments and clutter have remanent moments. This was the case for the

The first step in incorporating the instrument into the MTADS suite of sensors was to specify the temporal positions of the gates. The instrument can be configured in one of two modes—all four gates on the lower receive coil or one on the upper coil and three on the lower. In order to maintain backward compatibility of the data with the EM61 MkI data, we elected to use the second mode with the sampling gate on the upper coil and the first sampling gate on the lower coil at the same time as the MTADS EM61 MkI gates.

In order to gather the information required to make an intelligent choice for the later two gates in the MkII array, we leased an EM63 from Geonics for use at our Blossom Point Test Site. The EM63 can record the induced field decay in 26 time gates ranging out to beyond 20 milliseconds (ms). This instrument is not very amenable to vehicular use due to its low measurement rate, but it is ideal for accurately determining the complete decay response of test targets. We made measurements on the three projectiles expected to be encountered at the Badlands Bombing Range impact area—8-in, 155-mm, and 105-mm—as well as two frag clusters constructed by attaching pieces of frag recovered from the impact area in 1999 to styrofoam blocks to approximate the volume of the clusters encountered at the impact area.

An example of the data collected on a 105-mm projectile is shown in Figure 15. These data are eight of the time gates collected during a traverse over a horizontal 105-mm projectile 66 cm below the sensor. The results are color coded into two classes, red for data from the four decay times that correspond to the sampling gates used in the standard MkII with four gates on the lower coil, and blue for later gates. As shown in the figure, the shape of the response begins to change clearly only for decay times greater than 2 ms. This change in shape is the result of longer-lived modes beginning to predominate as the short-lived modes decay.

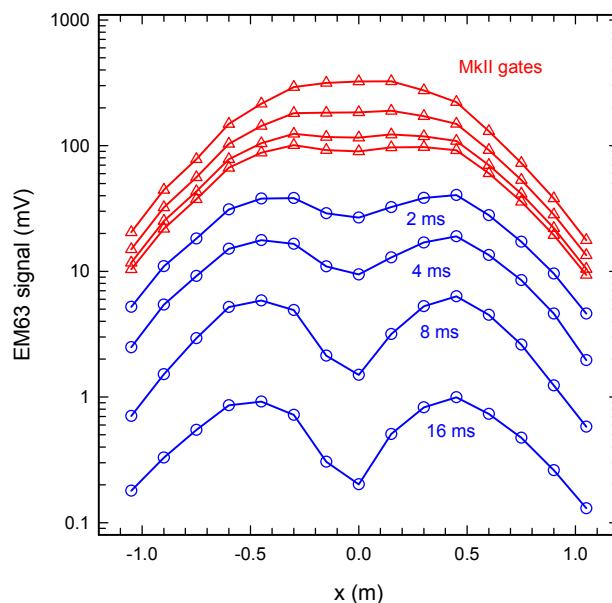


Figure 15. Measured EM63 Response Profiles at Eight Time Gates from a Traverse over a Horizontal 105-mm Projectile 66 cm below the Sensor.

Corresponding results for a frag cluster are shown in Figure 16. In this case, there is less variation of beta ratio with time, presumably because the measured response arises from the sum of many modes that decay with a range of decay times.

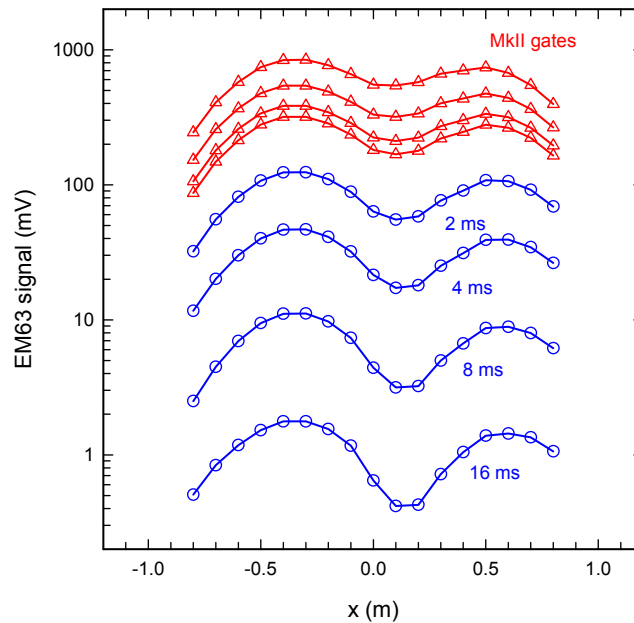


Figure 16. Measured EM63 Response Profiles at Eight Time Gates from a Traverse over a Frag Cluster.

Based on our measurements with the EM63, we initially specified a time for the latest gate in the MTADS EM61 MkII array of 2-5 ms. This number was a compromise between classification value which increases with increasing delay and signal to noise (S/N) which decreases as the antenna repetition rate is lowered to allow for later decay measurements. Unfortunately, due to some limitations of the design of their drive electronics, the latest gate Geonics could offer with an antenna repetition rate of 150 Hz was 1.2 ms. Rather than suffer the S/N consequences of lowering the repetition rate by a factor of 2, we settled for this relatively short gate for this demonstration. The actual gates available in the MTADS array for the two operating modes are listed in Table 7.

Table 7. Gate Times for the Two Modes of the MTADS EM61 MkIIs.

Operating Mode	“4 on lower”	“1 + 3”
Upper Coil – Gate 1		280-465 μ s
Lower Coil – Gate 1	280-465 μ s	280-465 μ s
Lower Coil – Gate 2	465-680 μ s	
Lower Coil – Gate 3	680-925 μ s	680-925 μ s
Lower Coil – Gate 4	925-1205 μ s	925-1205 μ s

4.2.2 Survey Data

A conventional MTADS magnetometer survey of the seed area was conducted as the first survey at the demonstration site. Following analysis using the MTADS Data Analysis System, 170 targets were marked for remediation. Following the practice of the Jefferson Proving Ground (JPG) V demonstration, the targets were classified using a 6-bin scheme, where category 1 corresponds to high confidence ordnance, category 2 is medium confidence ordnance, category 3 is low confidence ordnance, category 4 is low confidence clutter, category 5 is medium confidence clutter, and category 6 is high confidence clutter. The analysts attempted to scale their rankings such that digging all category 1–5 targets would completely clear UXO from the site. A summary of the analysis results is shown in Table 8. These results serve as a baseline against which to compare the performance of the EM61 systems as well as the MTADS airborne system.

Table 8. Summary of the Magnetometer Analysis Results.

Category	1	2	3	4	5	6	Total
Number of Targets	24	15	36	3	37	55	170

A North-South and an East-West EM61 MkII survey of the seed area were conducted as part of this demonstration as well as two orthogonal EM61 MkI surveys. A comparison of the results of the three surveys is shown for a small region of the Seeded Area in Figure 17.

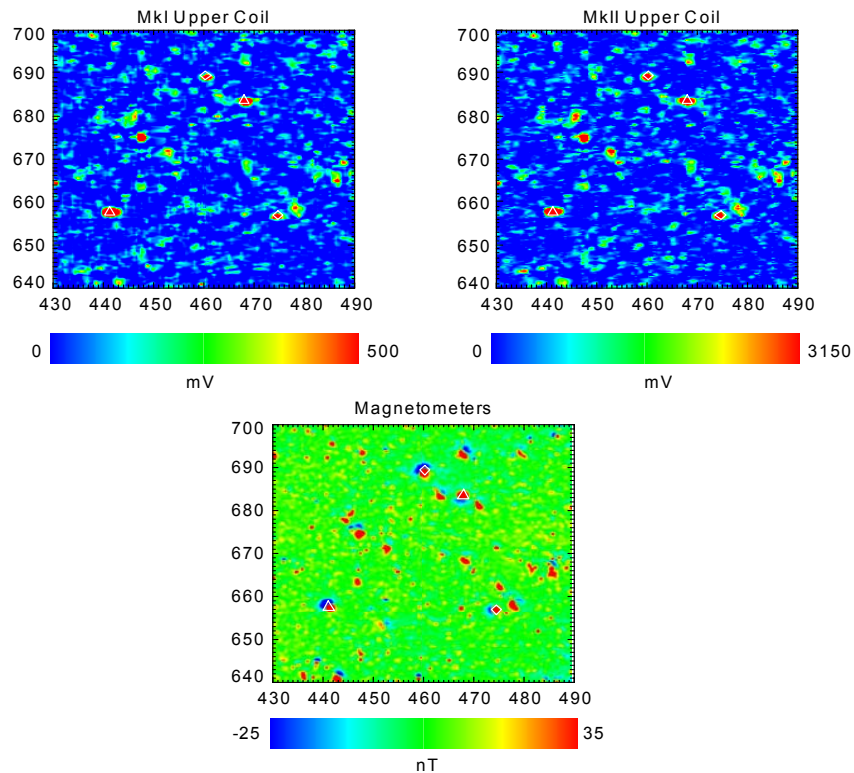


Figure 17. Comparison of Results from All Three Surveys of the Seeded Area in a Small Subgrid.
(The projectile targets are marked with diamonds for 105-mm and triangles for 155-mm.)

4.2.3 Data Assessment

4.2.3.1 EM61 MkII Electronic and Calibration Issues

During initial examination of the MkII survey data, we discovered several features that compromised our ability to achieve reliable model fits. Between time gates on a single MkII and among the three MkII sensors in the array, discrepancies were found in the gain factors, the sampling times, and the noise levels.

The MkII sensor measures the current in the transmit coil and uses this to normalize the output signal. This is done to maintain a constant output from the sensor as the battery voltage drops. When hooked up as an array of three sensors, one MkII is the master unit, and it triggers the two slave units. We initially noticed that the two slave sensors reported an odd oscillation of their transmit currents. Correcting the signal by these current variations caused their apparent signals to oscillate. Independent measurement of the transmit currents did not confirm these oscillations. In an array mode, the MkII sensors appear to have an electronic problem that causes an error in their current measurement circuitry. To correct for this, the current in the master sensor was used to normalize the signal in all three sensors. Even with this correction, problems were still observed with the relative outputs among the three sensors on the upper and lower coils and among the three time gates. A steel sphere was used as a calibration object to measure each sensor's response, and correction gain factors were found for each sensor and time gate. These correction factors were as large as 25% between sensors. There was some indication that these factors may have been changing day to day. The MkI array was similarly calibrated, but had only minor corrections (10% between sensors) and appeared to be consistent from day to day.

The MkI array was originally tested for timing problems between sensors by driving back and forth over a long wire or pipe. Each sensor was found to have a fixed timing offset needed to correctly map the data. Over time, these corrections have never been observed to vary. The same test with the MkIIs found similar timing offsets, but the offsets were found to vary from data file to data file. To correct for this, a "wire test" was performed in the field for each data file collected, and offsets were found for each file. Despite this added correction, there were still stretches of data collected where varying timing offsets were observed. The only conclusion is that the timing offsets change within a data file. Since the time of this demonstration, this sensor timing variation has been confirmed by other groups using the EM61 MkIIs.

Finally, from data file to data file and day to day, the noise levels on certain sensors and certain time gates has been observed to change. At times, the noise was as much as five times greater. This noise dominated short time scales and was present even when the sensors were stationary.

Given the inconsistent and unpredictable performance of the EM61 MkII discussed above, we must ask if there is enough new information in this sensor to justify the difficulty in using it. Figure 18 and Figure 19 show a comparison of the data collected by the EM61 MkII with that collected by the EM61 MkI over a high- and low-SNR 105mm projectile, respectively. In each of the figures, the upper coil signal is compared directly and the EM61 MkI lower coil signal is

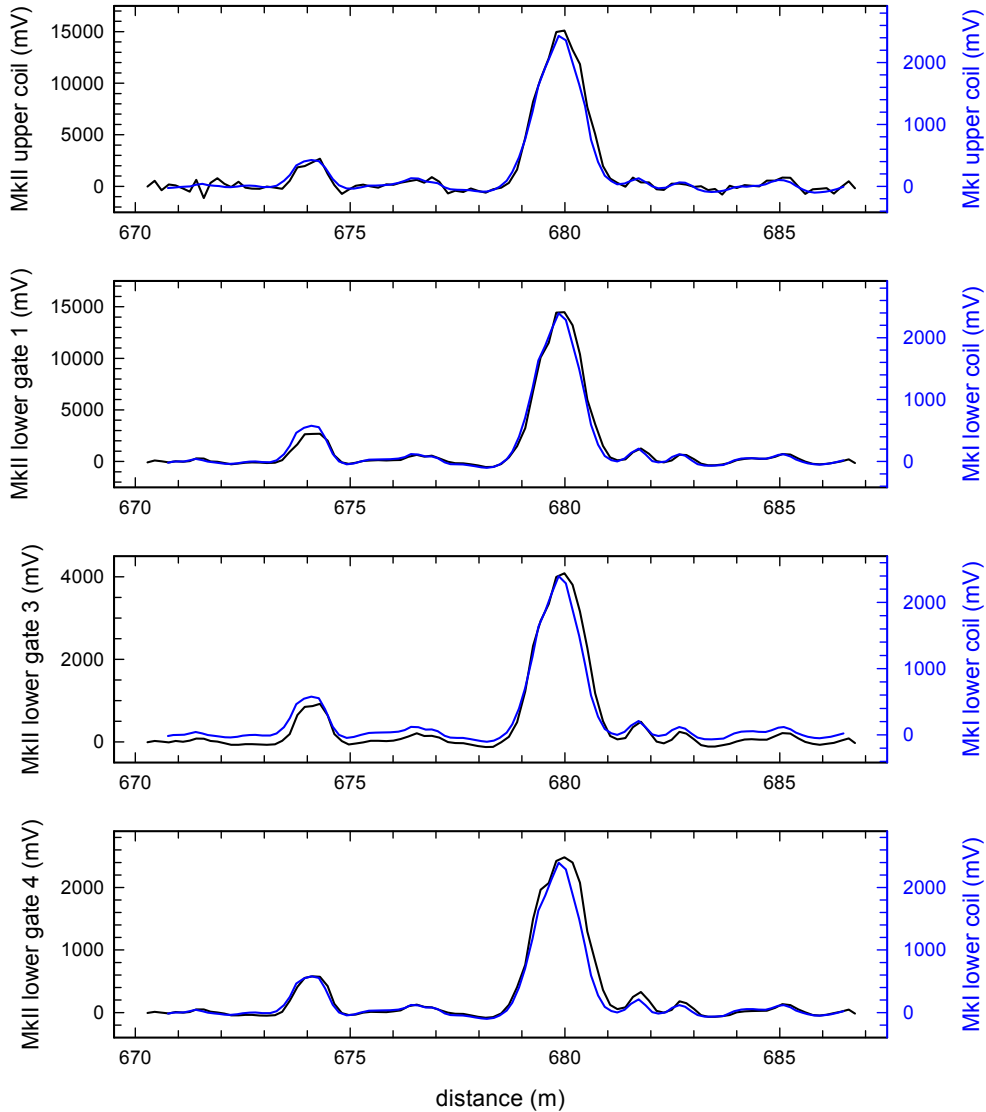


Figure 18. Comparison of the Signals from the EM61 MkII Array (Black) and the EM61 MkI Array (Blue) Arising from a High-SNR 105-mm Projectile.

compared to all three lower-coil gates. Since the gain is higher in the EM61 MkII, the signals to be compared have been scaled to be the same at the peak signal over the object.

As can be seen most clearly in the high-SNR example (but also in the low-SNR case) the signal in the later gates of the EM61 MkII is no different than that in the single lower coil gate in the EM61 MkI. We conclude that the EM61 MkII in the configuration used during this demonstration does not add significant classification capability to the MTADS system.

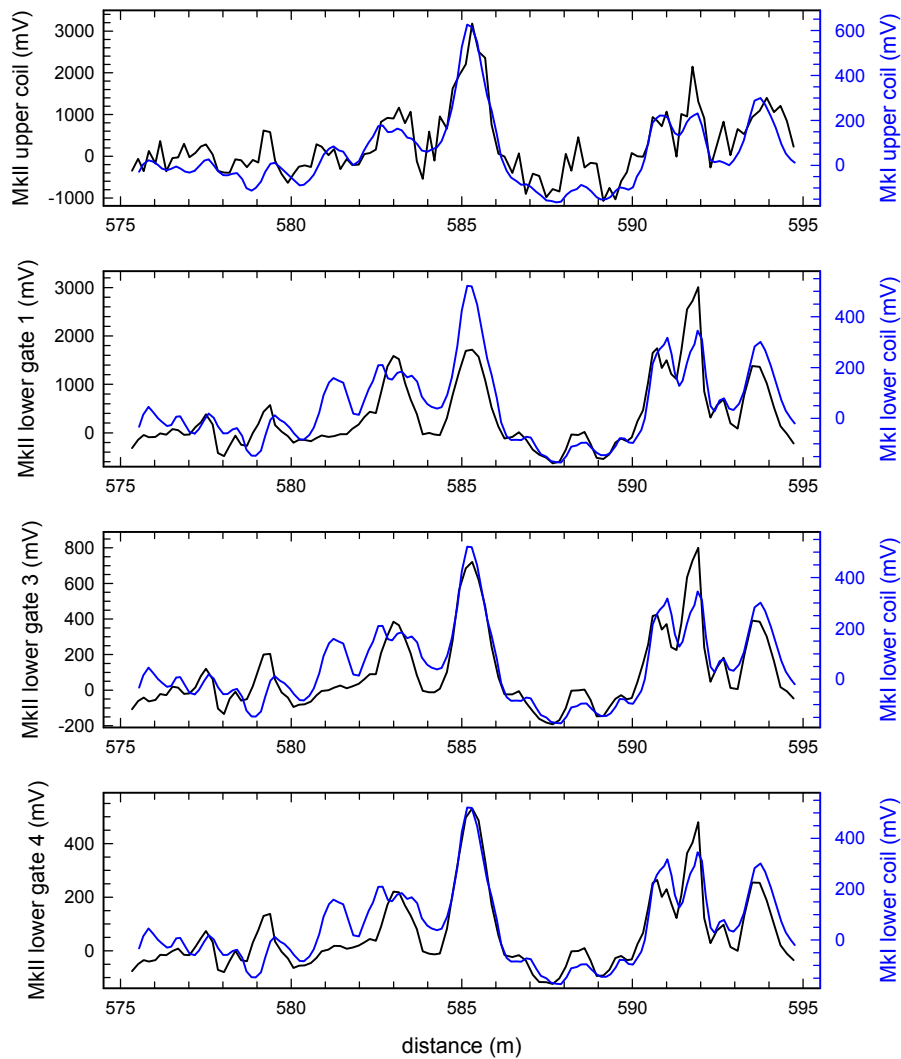


Figure 19. Comparison of the Signals from the EM61 MkII Array (Black) and the EM61 MkI Array (Blue) Arising from a Low-SNR 105-mm Projectile.

4.2.3.2 EM61 MkI Signal to Noise Ratios

Three data rasters illustrating the relative noise levels at the Blossom Point test site, the Blossom Point “L” Range, and the BBR seed area are shown in Figure 20. This plot confirms the relative noise levels seen with the MkII between the Blossom Point test site and the BBR. Figure 21 is a power spectral density plot for the data from those two sites.

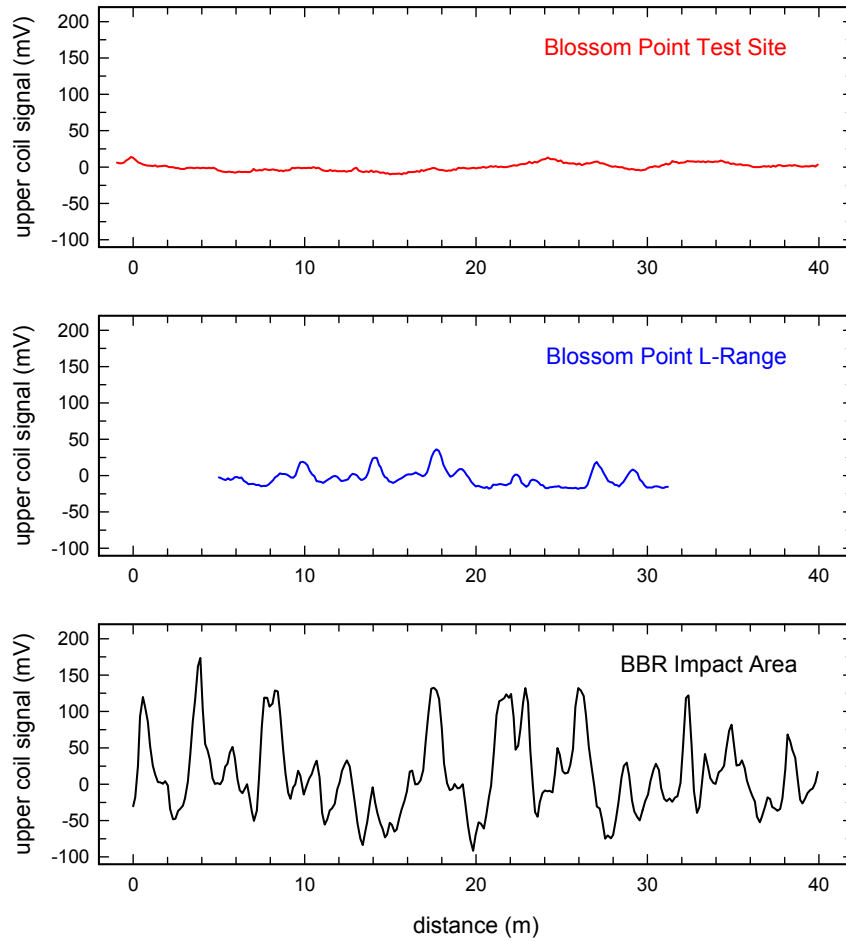


Figure 20. Comparison of the Noise Observed with the EM61 MkI at Three Sites.

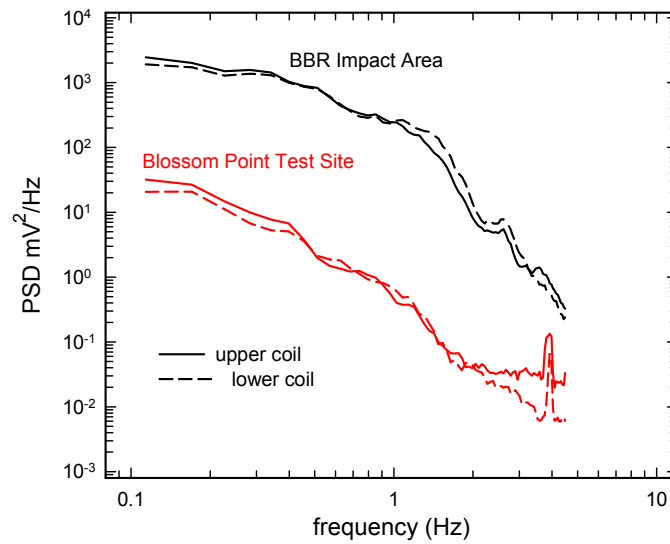


Figure 21. Power Spectral Density of the EM61 MkI Noise at Two Sites.

4.2.3.3 EM61 Model Fits

The original goal of this demonstration was to invert the data over each anomaly and, using the beta response coefficients, to identify each ordnance item and discriminate the ordnance from the clutter. In all, 70 anomalies exhibited signal amplitudes at least twice the background. The peak EMI signatures ranged in amplitude from 400 to 9,000 mV (arbitrary units from Geonics EM61). Background variation over the scale lengths of the anomalies (several meters) was on the order of 100-200 mV, which, as seen in Figure 24 is much greater than at other sites we have surveyed. Of the seeded ordnance, three 105-mm, and one 155-mm did not meet this S/N threshold. The missed 105-mm were deeper than 0.5 m. The missed 155-mm was 0.85-m deep. The 8-in ranged in depth from 0.3 m to 0.75 m. Of the 37 nonordnance items analyzed, there were 19 clusters of exploded fragments, 12 individual pieces of shrapnel, and six pieces of scrap metal from the auto bodies used as targets. The results for all fits discussed in this Section are listed in Appendix C.

The primary versus secondary fitted beta values for ordnance (left panel) and nonordnance (right panel) are shown in Figure 22. The symbols plot the primary beta value versus the average of the secondary values. The vertical line through each symbol indicates the maximum and minimum secondary beta values. Ideally for ordnance, the secondary beta values should be equal. The plotted circles are centered on the expected values for the betas of a 105-mm (solid), a 155-mm (dotted), and an 8-in (dashed). The circles are of equal radius on the log-log plots and in the left panel of Figure 22 contain all of the fitted ordnance items with a high S/N. These are shown with black symbols (105-mm as diamonds, 155-mm as squares, and 8-in as triangles). The red symbols in the left panel represent ordnance fits from low SNR data (peak signals less than 1,000 mV). These beta fits are far from the expected values. In the right panel of Figure 22, the symbols are green diamonds for fragment clusters, blue squares for single fragments, and pink triangles for scrap. The signals ranged in amplitude from 400 to 1,000 mV for the clusters, 500 to 2,000 mV for the singles, and 700 to 4,000 mV for the scrap. It should be noted that none of the nonordnance betas fall entirely within the high SNR ordnance spheres.

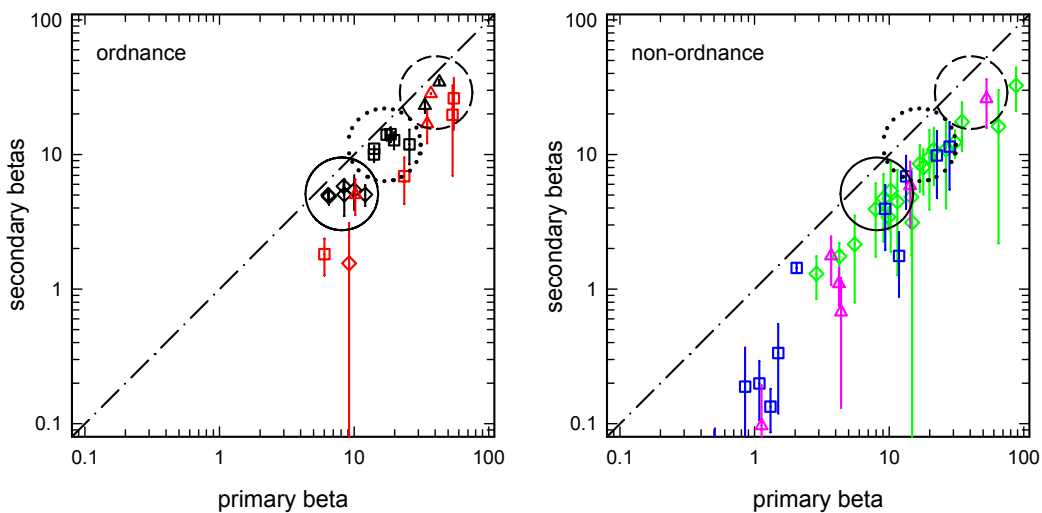


Figure 22. Plots of Primary Beta Versus Secondary Beta for Ordnance Items (left panel) and Clutter (right panel). (Circles represent regions containing high-SNR fits of the three ordnance types. See the text for an explanation of the symbols.)

In an effort to understand these low SNR fit results, both data/model fits and normalized chi-square surfaces for a high SNR 155-mm, a low SNR 155-mm, and a fragment cluster are shown in Figure 23, Figure 24, and Figure 25. The data rasters plot the measured data from the center sensor as it passes directly over the object. The black line is the data, the symbols are data used in the fit, and the colored lines represent the best model fit to the data. The chi-square surfaces are a function of primary beta value and depth below ground and have been normalized in each case to the minimum chi-square. In the high SNR case, Figure 23, the data and model fit very closely at a primary beta value of 14, and the curvature of the chi-square contours is very steep. For the low SNR case, Figure 24, the curvature is not as steep indicating a larger uncertainty in the fitted model parameters. Indeed, two model fits are shown in Figure 24, one at the minimum chi-square (red plots) with a beta value of 6.3 and one at a primary beta value of 14 (green plots). The differences between these two fits and the data are comparable to the signal variation due to noise. A major factor in these poor inversions is the simple EMI signal shape from large ordnance. Because of the small ratio of primary to secondary beta for large ordnance (~ 1.3), the signals are a simple single peak response, and large variations in depth and primary beta produce very similar signal shapes.

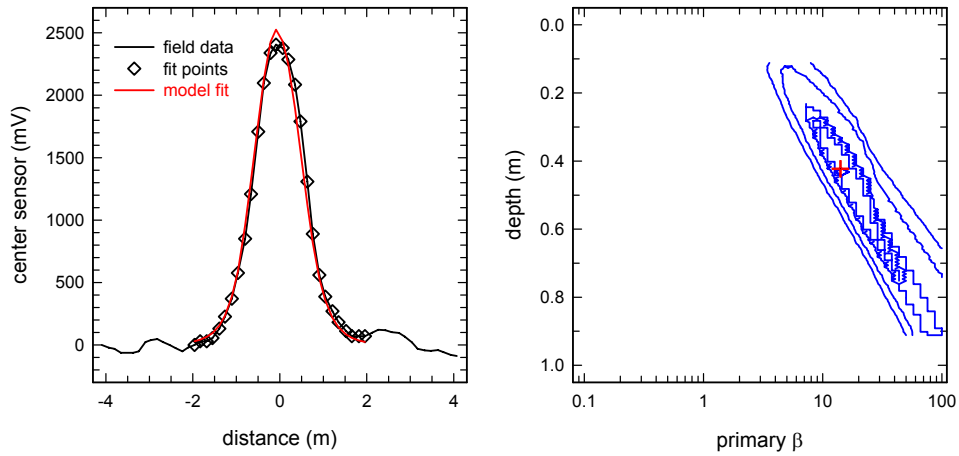


Figure 23. Data Fit and Chi-Square Contours for a High-SNR 155-mm Projectile.

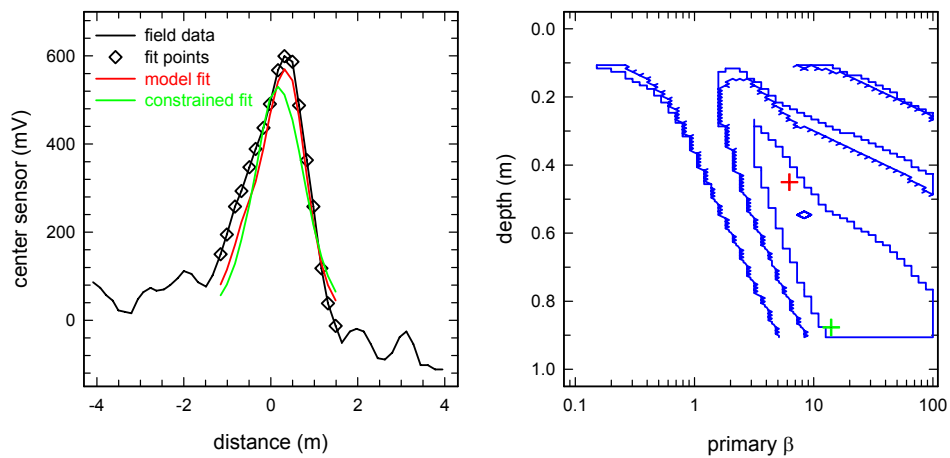


Figure 24. Data Fit and Chi-Square Contours for a Low-SNR 155-mm Projectile.

Fragment clusters on the other hand, as shown in Figure 25, produce a broader merged two peak structure and typically show these features in any survey direction. This constrains the model to two large horizontal betas and a small vertical beta ($\beta_x = \beta_y > \beta_z$). These are the betas expected from a flat axisymmetric plate.¹⁵ For this cluster, the betas were 12.5, 10.0, and 1.8. Even at low SNR, this two-peak structure remains significant, and the large spread in the secondary betas for all clusters can be seen in Figure 22. The normalized chi-square contours for this cluster are shown in the right panel of Figure 25. The curvature is not steep and the minimum is not well localized. This appears to be a result of the measured data simply not matching the model well no matter what the model parameters are. This poor match is not unexpected given that the signal comes from the sum of a number of small objects spread out over an area and not a single distinct metal object, which is what the model is based on.

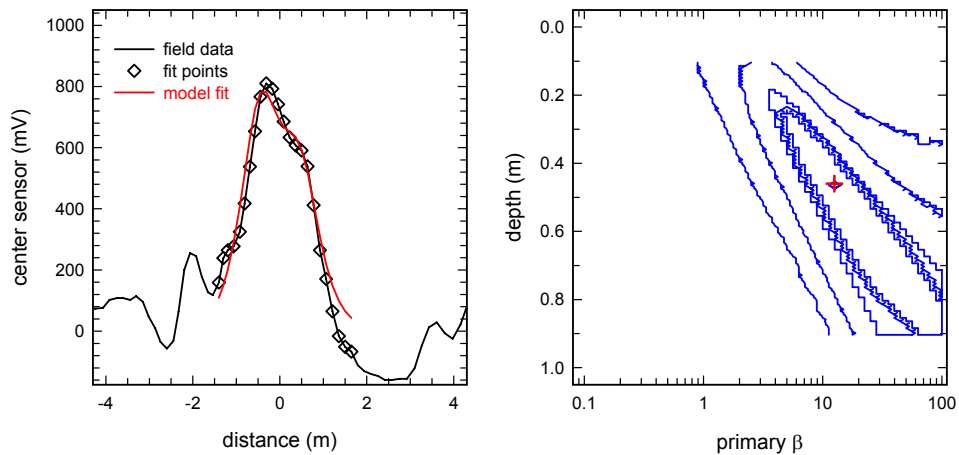


Figure 25. Data Fit and Chi-Square Contours for a Frag Cluster.

4.2.3.4 An Alternate Discrimination Approach

The consistent poor match between data and model for nonordnance fragment clusters suggests using a goodness-of-fit metric as a means of discriminating between ordnance and clutter. After considering several, the reduced chi-square was found to be an effective discriminant. For each fit, this quantity was calculated as the sum of the difference between model and data squared divided by the standard deviation of the noise squared and divided by the number of degrees of freedom. The noise was assumed to be roughly Gaussian with a standard deviation of 100 mV. Simple distributions of the background showed this only to be approximately true. The reduced chi-square as a function of peak signal for ordnance (left panel) and non-ordnance (right panel) is plotted in Figure 26. The colors and symbols denote the same items as in Figure 22. The dotted line denotes a straightforward means of discrimination by considering the ratio of the reduced chi-square to the peak signal.

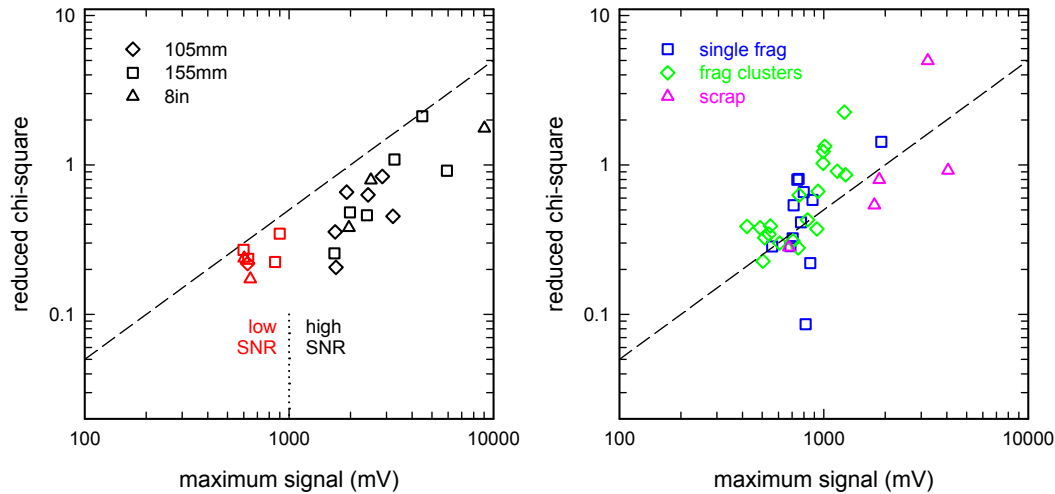


Figure 26. Plots of Reduced Chi-Square Versus Peak Signal for Ordnance (Left Panel) and Clutter (Right Panel). (The dashed line scales linearly with signal and indicates a rough threshold to separate ordnance from clutter. The symbols are the same as those in Figure 25.)

The “beta sphere” method of discrimination is compared to this “goodness-of-fit” method in Figure 27. For the beta sphere approach, the three dimensional distance of the logarithm of the three fitted betas from the expected logarithm of the betas for the three ordnance items is calculated, and the minimum distance is kept for each. This beta distance is plotted as a function of object type in the upper panel of Figure 27, and again the colors and symbols are the same as in Figure 22. Note, except for an 8-inch target that fit very close to the expected 105-mm betas, that all of the low SNR ordnance values are anomalously large and all of the high SNR values are reasonably distinct from the clutter. In the lower panel of Figure 27, the reduced chi-square divided by the peak signal is plotted as a function of object type. At a level that picks up all of the ordnance, this chi-square quantity only picks up a modest number of non-ordnance. This is quite an improvement over the beta sphere method in separating ordnance from clutter.

A further improvement on this discrimination was found by constraining the beta fits to the expected beta values for each ordnance type. Each target was fitted with the beta values for a 105-mm (8.8, 5.1, 5.1), a 155-mm (16.8, 11.8, 11.8), and an 8-in (40.6, 28.8, 28.8). The fit with the lowest chi-square was kept. The resulting primary beta as a function of target type is plotted in the upper panel of Figure 28. Curiously, actual 105-mm fit equally to 105-mm betas and 155-mm betas; the 155-mm fit to all three betas; the 8-in fit to 155-mm and 8-inch betas. The clutter fits almost equally to all three ordnance betas. In the lower panel of Figure 28, the reduced chi-square from the constrained fitting is divided by peak signal and plotted as a function of object type. For this discriminant, all the ordnance can be separated from all but four clutter items.

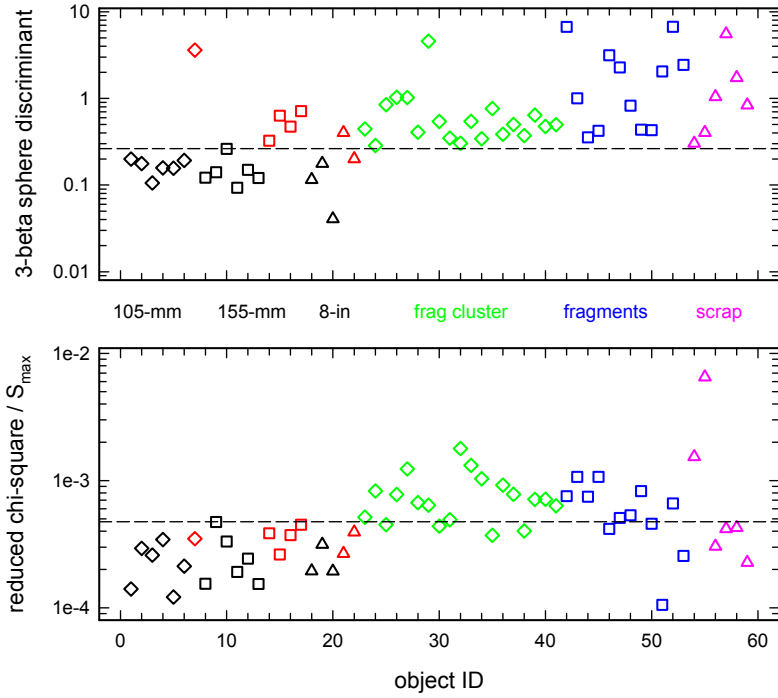


Figure 27. Comparison of the Beta Sphere Discriminant to the Goodness-of-Fit Discriminant.

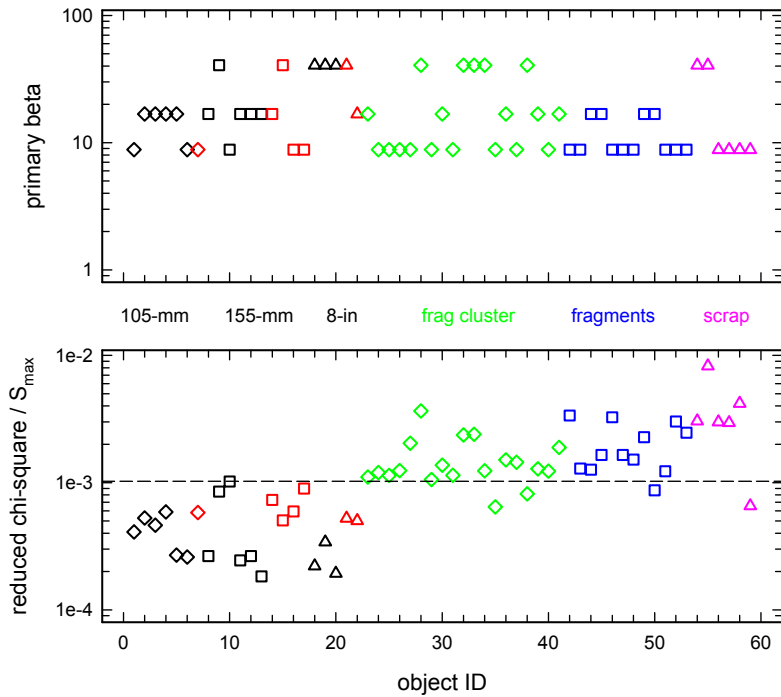


Figure 28. Results of the Constrained Fits.

The ROC curves in Figure 29 compare the relative performance of these three methods. As the three discriminant levels are varied, the number of ordnance items correctly identified as ordnance (probability of detection) is plotted against the number of nonordnance items incorrectly identified as ordnance (probability of false alarm). The goodness-of-fit discriminant based on the constrained beta fits provides the best overall performance.

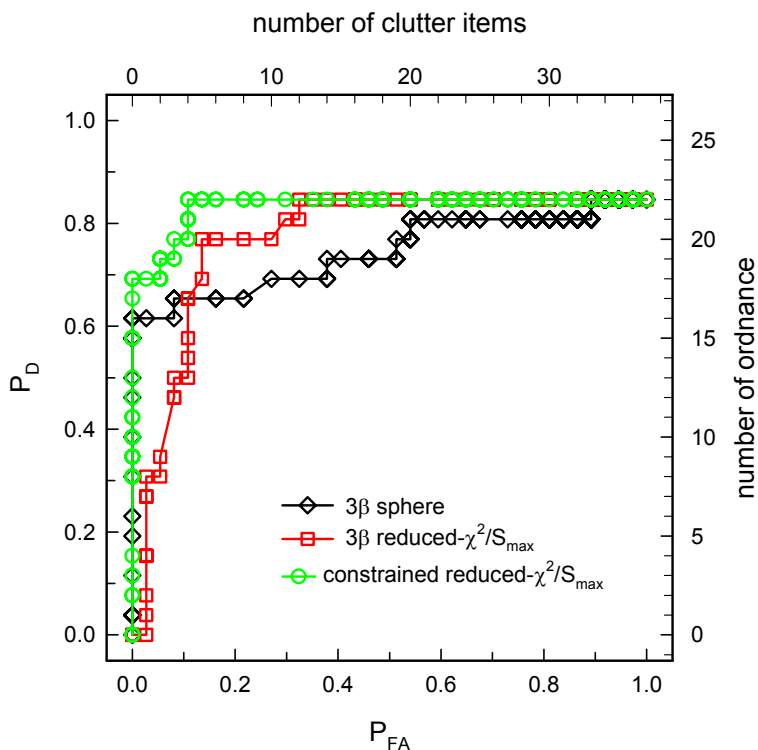


Figure 29. ROC Curves Comparing the Discrimination Performance of the Three Methods.

4.2.3.5 Technology Comparison

The previous section showed the results of our analysis of the EM results obtained during the Impact Area survey and demonstrated in Figure 29 that the normalized χ^2 from a constrained beta fit is the most effective discriminant. The baseline technology for comparison of these results is magnetometry. As mentioned in the Introduction, we have had considerable discrimination success when a skilled analyst fits magnetic anomalies and classifies the resulting targets. The magnetometry targets were categorized using the 6-bin priority (or confidence) scheme first introduced at JPG V and discussed above. The magnetometer data analysts attempted to scale their rankings such that digging all targets in categories 1-5 would clear all UXO from the site.¹⁹ The model parameters resulting from the magnetometry analysis were also submitted to the PNN developed in the NRL/Blackhawk SERDP program. This neural net was trained using test pit measurements on the three ordnance types emplaced in the seed area. Figure 30 shows a set of ROC curves comparing the performance of the constrained beta fit discriminant with those of the two magnetometry analyses. In contrast to Figure 29,

the abscissa of this plot is false alarms per hectare. Since the two methods detected a different number of objects, this is the only way to make a meaningful comparison.

The most obvious point from Figure 30 is that the EMI system detected only 22 of the 26 ordnance items in the seed area. As discussed above, this is a function of the high noise in the EMI survey data. This noise arises from the near-saturation coverage of small frag pieces on this site to which the EMI system is much more sensitive. One obvious way to reduce this frag problem is to collect data at later times, after the contribution from the small frag pieces has decayed away. We discussed above the reasons this approach is not possible with the standard EM61 MkII that we deployed for this demonstration.

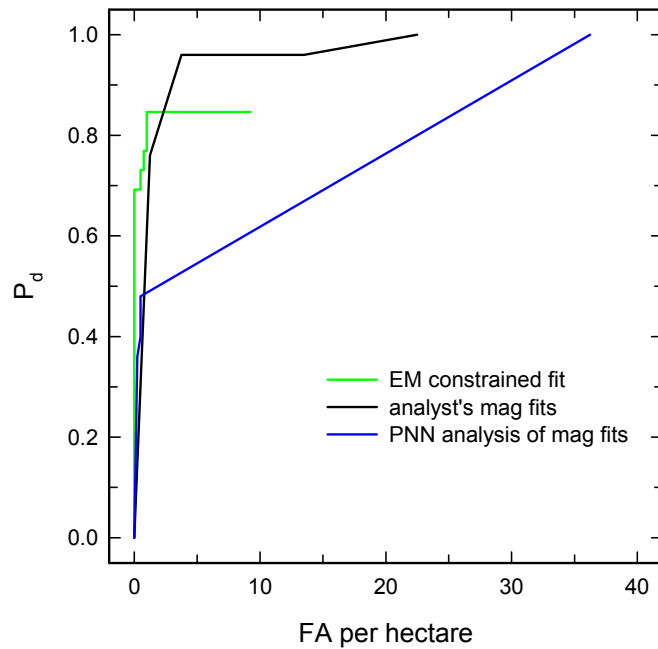


Figure 30. ROC Curves Comparing the Discrimination Performance of the Constrained Beta Fit with the Two Magnetometry Analyses Used in this Demonstration.

This page left blank intentionally.

5.0 COST ASSESSMENT

5.1 COST ANALYSIS

The estimated costs for an MTADS EM survey in two orthogonal directions and the data analysis required to implement the model described here for a hypothetical 200-acre survey are listed in Table 9 along with an estimate for a mag-and-flag survey of the same area. For neither survey do we assume remediation of targets. The MTADS survey has been carried through target analysis providing target maps and target tables with position size and depth of all targets. The mag-and-flag survey is assumed to flag each target as it is detected and later survey the flags for archival purposes.

Table 9. Cost Comparison for a Hypothetical 200-Acre Survey Using These Methods.

Expense		MTADS EM Survey 25 Survey Days		Mag-and-flag 14 Field Days	
Labor Category	Burdened Rate (\$/hr)	#	Total \$	#	Total \$
Site supervisor	\$100	1	\$ 20,000		
UXO site supervisor	\$70			1	\$ 7,840
Data analyst	\$60	1	\$ 12,000		
UXO supervisor	\$60	1	\$ 12,000	2	\$ 13,440
HAZWOPR-trained staff	\$25	1	\$ 5,000		
UXO specialists	\$30			8	\$ 26,880
Local field support	\$20	4	\$ 16,000		
Total Labor Cost			\$ 65,000		\$ 48,160
Travel @ \$1,000/person			\$ 4,000		\$ 11,000
Hotel @ \$75/day			\$ 9,900		\$ 14,850
Per diem @ \$45/day			\$ 5,940		\$ 8,910
Logistics			\$ 40,000		\$ 3,000
Amortization @ \$100/survey hour			\$ 20,000		
Surveying flagged targets for GIS					\$ 30,000
Total Survey Cost			\$144,840		\$115,920

Based on our experience in supporting and using the MTADS at previous demonstrations, we propose to amortize \$400,000 of the MTADS hardware costs based on a schedule of 4,000 hours of surveys.¹² This is a conservative estimate based on breakage, maintenance, and replacement costs for the past 4 years.

In our experience with MTADS at field operations, we have always had one senior scientist/supervisor on site supporting the operation. We have provided extensive logistics support such as tents for maintenance work, offices with bench spaces for repairs, and on-site office spaces for computers and DAS support equipment. It is our experience that these support elements have a positive impact on our survey efficiency, the quality of data collected, and the on-site analysis product. For this reason, we use the same support and logistics costs for the comparison purposes. A commercial firm in a cost-competitive environment might forgo some of these logistics costs.

The MTADS survey costs include two orthogonal EM surveys only; no magnetometer survey is included. If large, deep targets were expected, a magnetometer survey would be required and an additional \$50,000 would be necessary. Since two orthogonal EM surveys are included in the estimate while only one would be required for target detection, the added cost of these methods is \$300 per acre. This is almost equal to the costs required to remediate one or two targets per acre. Thus, the economic break even point for the use of these methods is reached when three false alarms per acre are avoided.

For the mag-and-flag operations, we assume that the number of personnel put on site is the number that can complete the survey in a 3-week period of performance. This minimizes the travel and logistics costs. The labor mix of UXO technicians to UXO supervisors and the site supervisor support and logistics support are typical of those that we have had quoted to support operations and also factor in information about labor rates and labor mixes typically quoted for operations similar to these.

5.2 COST COMPARISON

These calculations, which show that the methods demonstrated here are 25% more costly on a per acre basis, do not address the ultimate goal of a particular survey: Is the survey being conducted to support remediation activities, or simply to provide an indication of whether the site is contaminated and the extent of the ordnance contamination? Previous studies of the detection efficiencies of mag-and-flag operations (at least for sites where ordnance exists below 1 meter in depth) have shown that most of ordnance remains undetected.

Assuming that the survey is in support of a remediation activity, the cost per detected target is a useful comparison. Using documented mag-and-flag detection efficiencies of 35%,¹ we find that these methods are more than twice as cost efficient at flagging ordnance for remediation. It should also be noted that following remediation based on a mag-and-flag survey 65% of the ordnance targets remain in the ground. Even these numbers do not take into account the false alarm reduction demonstrated in this survey. In the worst-case scenario, discriminating ordnance ranging from fuzes to 5-in shells from scrap, we were able to reject >20% of the false alarms without missing an ordnance target. With a more restricted target set, false alarm reductions of 33-50% are possible. Since a mag-and-flag survey has no significant classification ability, all targets have to be remediated.

The true cost comparison of interest is a comparison of the results demonstrated by this method versus the baseline MTADS magnetometry analysis. A preliminary version of this comparison was attempted in the fall of 1999 at the Badlands Bombing Range impact area.¹⁸ The analysis described here was able to reject a number of false alarms that would have been marked for digging by the magnetometer analysis. The comparison is incomplete, however, as there was only one ordnance item detected in the area surveyed by the EM array. The second demonstration described here was undertaken to address this uncertainty. As shown in Figure 30, the initial slope of the ROC curve for our EM analysis is slightly steeper than the corresponding curve for the magnetometer analysis. This early advantage for these methods is overcome, however, by the fact that the EM system was able to achieve a high enough signal-to-noise ratio for reliable models fits for only 22 of the 26 ordnance items in the seed area.

6.0 REFERENCES

1. "Hand-held Gradiometer Survey Test at The Marine Corps Air Ground Combat Center, Twentynine Palms, CA," NAVEODTECHCEN TR, September 1992.
2. "MTADS TECHEVAL Demonstration, October 1996," H. H. Nelson, J. R. McDonald, and Richard Robertson, NRL/PU/6110--97-348.
3. "Results of the MTADS Technology Demonstration #2, Magnetic Test Range, Marine Corps Air Ground Combat Center, Twentynine Palms, CA, December 1996," J. R. McDonald, H. H. Nelson, R. A. Jeffries, and Richard Robertson, NRL/PU/6110--97-349.
4. "Results of the MTADS Technology Demonstration #3, Jefferson Proving Ground, Madison, IN, January 13-24, 1997," H. H. Nelson, J. R. McDonald, R. A. Jeffries, and Richard Robertson, NRL/PU/6110--99-375.
5. "MTADS Unexploded Ordnance Operations at the Badlands Bombing Range, Pine Ridge Reservation, Cunny Table, SD, July 1997," J. R. McDonald, H. H. Nelson, J. Neece, Richard Robertson and R. A. Jeffries, NRL/PU/6110--98-353.
6. "MTADS Demonstration at the Former Fort Pierce Amphibious Base, Vero Beach, FL, March 1998," J. R. McDonald, H. H. Nelson, R. A. Jeffries, Richard Robertson, and K. Blankinship, NRL/PU/6110--98-372.
7. "MTADS Live Site Survey, Bombing Target #2 at the Former Buckley Field, Arapahoe County, CO," J. R. McDonald, H. H. Nelson and R. Robertson NRL/PU/6110--99-379.
8. "MTADS Geophysical Survey at The Jamaica Island and Topeka Pier Landfills at The Portsmouth Naval Shipyard, Kittery, ME, October 1998," J. R. McDonald, H. H. Nelson and B. Puc, NRL/PU/6110--99-381.
9. "MTADS Live Site Demonstration, Pueblo of Laguna, 6 July—7August 1998," J. R. McDonald, H. H. Nelson and R. A. Jeffries NRL/PU/6110--00-398.
10. "MTADS UXO Survey and Remediation on the Walker River Paiute Reservation, Schurz, NV, November 1998," J. R. McDonald, H. H. Nelson, and R. A. Jeffries NRL/PU/6110--00-406.
11. "MTADS Geophysical Survey of Potential Underground Storage Tank Sites at the Naval District Washington, Anacostia Annex," H. H. Nelson, J. R. McDonald, R. Robertson, and B. Puc, NRL/MR/6110--00-8435.
12. ESTCP Cost and Performance Report. *Multi-Sensor Towed Array Detection System*. September 1999. <http://www.estcp.org/documents/techdocs/199526.pdf>.

13. "Collection and Analysis of Multi-sensor Ordnance Signatures with MTADS," Bruce Barrow and H. H. Nelson, *J. Environ. Engineering Geophysics*, **3**, 71 (1998).
14. "Model-Based Characterization of EM Induction Signatures for UXO/Clutter Discrimination Using the MTADS Platform," Bruce Barrow and H. H. Nelson, Proceedings of the UXO Forum 1999, Atlanta, GA, May 25-27, 1999.
15. "Model-Based Characterization of EM Induction Signatures Obtained with the MTADS EM Array," Bruce Barrow and H. H. Nelson, *IEEE Trans. Geophys. Remote Sens.*, **39**, 1279 (2001).
16. "MTADS Unexploded Ordnance Operations at the Badlands Bombing Range Air Force Retained Area, Pine Ridge Reservation, SD, September, 1999," J. R. McDonald, H. H. Nelson, Richard Robertson and R. A. Jeffries, NRL/PU/6110--00-424.
17. "Draft Final Removal Report: Ordnance Removal at Army Research Laboratory, Blossom Point Field Test Facility (BPFTF), Blossom Point, Maryland," Human Factors Applications, Inc., DACA87-95-D-0027, Task Order 0008, 18 April 1997.
18. "Electromagnetic Induction and Magnetic Sensor Fusion for Enhanced UXO Target Classification," H. H. Nelson and Bruce Barrow, NRL/PU/6110--00-423.
19. "Airborne MTADS Demonstration on the Impact Area of the Badlands Bombing Range, September 2001," J. R. McDonald, David Wright, Nagi Khadr, and H. H. Nelson, NRL/PU/6110--02-453.

APPENDIX A

POINTS OF CONTACT

Point of Contact	Organization	Phone/Fax/E-mail	Role in Program
Dr. Jeffrey Marqusee	ESTCP	703-696-2120 703-696-2114 jeffrey.marqusee@osd.mil	ESTCP Director
Dr. Anne Andrews	ESTCP	703-696-3826 703-696-2114 anne.andrews@osd.mil	Program Manager, UXO
Jeffrey Fairbanks	ESTCP	703-736-4514 703-471-4180 jef@hgl.com	Program Assistant for UXO
Dr. Herbert Nelson	Naval Research Laboratory Washington, DC	202-767-3686 202-404-8119 herb.nelson@nrl.navy.mil	Principal Investigator
Mr. Jack Kaiser	Army Research Laboratory, Blossom Point	301-870-2329 301-870-3130 jkaiser@arl.mil	Blossom Point Site Manager
Mr. Bill Davis	Army Research Laboratory, Blossom Point	301-394-2434 301-394-2514 wdavis@arl.mil	Explosives Safety Officer
Dr. Dan Steinhurst	Nova Research, Inc. Alexandria, VA	202-767-3556 202-404-8119 das@ccs.nrl.navy.mil	Project Scientist
Mr. Glenn Harbaugh	Nova Research, Inc. Alexandria, VA	301-392-1702 301-870-3130 glennqueld@aol.com	Site Safety Officer
Dr. Tom Bell	AETC, Inc. Arlington, VA	703-413-0500 703-413-0505 tbell@va.aetc.com	Project Manager
Dr. Bruce Barrow	AETC, Inc. Arlington, VA	703-413-0500 703-413-0505 bjb@va.aetc.com	Project Scientist
Dr. J. R. McDonald	AETC, Inc. Raleigh, NC	919-653-0215 919-653-0219 jimrmcdonald@nc.rr.com	Project Scientist

This page left blank intentionally.

APPENDIX B

**MTADS TARGET REPORT FROM THE L RANGE
DEMONSTRATION**

This page left blank intentionally.

Appendix B. MTADS Target Report from the L Range Demonstration.

Target #	Mag Local X (m)	Mag Local Y (m)	Mag Depth (m)	3β Local X (m)	3β Local Y (m)	3β EM Depth (m)	Mag Size (m)	Mag Moment	Fit Quality	β1	β2	β3	Theta	Phi	Psi	χ ²	3β Coherence	Remediation Results
FUS-1	184.40	106.05	0.09	184.34	106.1	0.05	0.037	0.027	0.977	0.78	0.34	0.46	8	-64	-93	1110.4	0.967	Frag
FUS-2	175.73	125.13	0.07	175.57	125.29	0.03	0.035	0.023	0.981	0.39	0.04	0.11	-69	-136	18	808.1	0.969	Frag
FUS-3	164.98	135.15	0.10	164.92	135.18	0.11	0.098	0.515	0.950	1.84	0.31	0.60	-10	123	-41	1349.4	0.968	Frag
FUS-4	158.60	135.47	0.53	158.53	135.49	0.36	0.134	1.312	0.961	10.81	6.77	7.89	20	-171	-121	3841.0	0.988	Frag
FUS-5	170.89	134.25	0.16	170.85	134.38	0.12	0.040	0.035	0.965	1.93	0.54	0.30	11	-168	-117	1306.6	0.965	Nonordnance
FUS-6	158.13	145.54	0.45	158.42	145.46	0.37	0.083	0.311	0.943	4.99	1.64	1.86	-31	151	-165	1081.8	0.971	81-mm mortar
FUS-7	153.48	141.09	0.24	153.76	141	0.11	0.070	0.189	0.943	0.55	0.45	0.39	-30	135	132	651.0	0.948	Ordnance-related
FUS-8	151.64	180.20	0.09	151.7	180.13	0.19	0.026	0.010	0.902	1.79	0.35	0.66	32	107	-34	1268.9	0.964	Frag
FUS-9	138.88	202.80	0.17	138.97	202.79	0.06	0.092	0.427	0.959	0.25	0.17	0.23	-1	-40	-166	305.2	0.950	Nonordnance
FUS-10	143.19	120.06	0.12	143.28	120.16	0.14	0.036	0.026	0.962	0.96	0.33	0.62	-3	44	148	1335.6	0.937	Ordnance-related
FUS-11	138.90	163.80	0.08	138.86	163.78	-0.02	0.080	0.279	0.992	0.13	0.03	0.06	-4	-121	-89	70.8	0.949	Frag
FUS-12	142.93	153.88	0.18	143.34	153.86	0.19	0.072	0.206	0.914	0.93	0.17	0.58	-8	26	82	435.8	0.852	Frag
FUS-13	146.36	194.07	0.01	146.13	194.5	0.13	0.032	0.018	0.980	0.80	0.12	0.45	-28	179	87	844.3	0.913	Frag
FUS-14	130.02	163.44	0.50	129.91	163.41	0.48	0.077	0.250	0.967	3.37	1.71	1.55	-63	69	146	504.6	0.972	81-mm mortar
FUS-15	128.37	154.60	0.07	128.18	155.19	0.09	0.095	0.470	0.993	0.95	0.60	0.29	5	-84	11	967.3	0.940	Frag
FUS-16	132.61	150.66	0.09	132.72	151.07	0.08	0.083	0.311	0.992	0.71	0.04	0.14	-7	53	-95	336.1	0.929	Frag
FUS-17	123.03	132.85	0.10	123.06	132.89	0.02	0.047	0.055	0.898	0.73	0.02	0.07	-24	88	-155	787.4	0.968	Frag
FUS-18	123.87	189.98	0.10	123.77	190.09	0.02	0.031	0.016	0.964	0.32	0.02	0.00	58	-71	-5	355.5	0.965	Frag
FUS-19	124.10	112.56	0.05	124.01	112.57	0.03	0.049	0.062	0.992	0.62	0.03	0.00	4	-163	82	418.2	0.931	Nonordnance
FUS-20	116.29	155.73	0.63	116.58	155.89	0.33	0.288	13.033	0.925	12.13	7.03	3.92	-2	62	40	7002.8	0.953	Nonordnance
FUS-21	119.36	159.32	0.12	119.3	159.28	0.06	0.035	0.024	0.811	0.67	0.46	0.33	46	-9	83	738.6	0.975	Cone-shaped warhead
FUS-22	114.89	162.38	0.07	114.87	162.38	0.02	0.029	0.013	0.970	0.21	0.03	0.05	-10	-120	-127	83.3	0.919	Frag
FUS-23	112.19	168.08	0.53	112.18	168.07	0.21	0.342	21.740	0.953	4.41	2.53	1.25	-12	-152	-72	1719.8	0.985	Nonordnance
FUS-24	113.05	171.41	0.13	113.12	171.41	0.14	0.044	0.047	0.892	1.67	0.25	0.96	-2	-155	-100	1337.1	0.917	Nonordnance
FUS-25	99.69	158.16	0.32	99.69	158.16	0.02			0.971	0.41	0.14	0.01	80	92	106	613.0	0.971	Nonordnance
FUS-26	89.48	141.77	0.09	89.55	141.83	0.03	0.033	0.019	0.858	0.45	0.37	0.33	-8	169	-45	477.1	0.982	Ordnance-related
FUS-27	96.67	144.71	0.55	96.97	144.46	0.52	0.082	0.303	0.989	9.02	3.00	5.18	-37	80	-114	1126.0	0.961	Projectile with frag sleeve
FUS-28	101.99	148.81	0.49	101.99	148.81	0.19			0.939	0.64	0.04	0.43	-2	70	176	664.6	0.939	Frag
FUS-29	91.48	122.56	0.11	91.5	122.66	0.03	0.037	0.027	0.887	0.30	0.19	0.26	42	20	124	367.5	0.972	Ordnance-related
FUS-30	104.61	109.57	0.16	104.71	109.49	0.13	0.058	0.107	0.906	1.08	0.84	0.70	-10	-37	-13	1398.7	0.964	Ordnance-related
FUS-31	102.79	105.80	0.16	102.7	105.76	0.07	0.060	0.118	0.837	5.08	1.55	1.26	5	30	69	3324.5	0.980	76mm mortar
FUS-32	94.74	102.22	0.66	94.5	102.34	0.36	0.091	0.414	0.981	2.90	1.79	1.25	40	154	-26	590.2	0.969	81-mm mortar
FUS-33	79.25	96.98	0.13	79.2	97.04	0.08	0.041	0.038	0.939	1.32	0.15	0.19	-2	-77	159	265.7	0.975	Ordnance-related
FUS-34	82.35	109.49	0.11	81.71	109.54	0.17	0.059	0.109	0.948	0.87	0.10	0.06	-23	36	110	260.8	0.929	Frag
FUS-35	78.17	141.27	0.13	77.98	141.26	0.14	0.041	0.036	0.920	0.77	0.54	0.10	-10	95	172	341.9	0.929	Frag

Appendix B. MTADS Target Report from the L Range Demonstration (continued).

Target #	Mag Local X (m)	Mag Local Y (m)	Mag Depth (m)	3β Local X (m)	3β Local Y (m)	3β EM Depth (m)	Mag Size (m)	Mag Moment	Fit Quality	β1	β2	β3	Theta	Phi	Psi	χ2	3β Coherence	Remediation Results
FUS-36	76.38	139.16	0.26	76.39	138.96	0.24	0.048	0.060	0.791	1.06	0.24	0.52	-12	-65	-85	250.3	0.928	Frag
FUS-37	79.93	138.19	0.13	79.59	138.34	0.26	0.032	0.019	0.789	1.15	0.56	0.42	-4	-111	180	116.1	0.969	Frag
FUS-38	80.56	141.07	0.41	80.7	141.04	0.22	0.036	0.026	0.829	0.86	0.52	0.17	-16	35	29	197.9	0.956	Frag
FUS-39	76.19	165.19	0.17	76.12	165.24	0.11	0.046	0.052	0.972	1.23	0.23	0.18	6	100	163	517.7	0.962	Frag
FUS-40	81.68	165.59	0.03	81.73	165.57	0.12	0.089	0.388	0.933	0.80	0.41	0.19	-11	77	33	444.1	0.953	Frag
FUS-41	84.51	169.42	0.50	84.51	169.32	0.34	0.264	9.999	0.946	4.97	0.83	1.47	25	-127	-160	806.3	0.950	Nonordnance
FUS-42	77.58	179.65	0.54	77.75	179.5	0.39	0.086	0.340	0.963	3.13	1.11	1.67	31	6	166	1248.8	0.950	81-mm mortar
FUS-43	75.70	178.83	0.12	75.45	179.18	0.29	0.037	0.029	0.857	1.38	0.25	0.45	7	-55	14	359.5	0.915	Nonordnance
FUS-44	83.78	181.19	0.45	83.46	181.3	0.40	0.094	0.457	0.939	7.25	1.78	2.56	21	147	57	866.6	0.968	81-mm mortar
FUS-45	77.82	183.79	0.06	77.81	183.76	0.04	0.071	0.197	0.929	0.32	0.01	0.00	5	-62	-116	115.7	0.935	Frag
FUS-46	59.75	173.51	0.78	59.8	173.75	0.53	0.095	0.467	0.948	4.41	2.55	1.74	54	73	6	239.2	0.986	81-mm mortar
FUS-47	73.18	153.65	0.24	73.19	153.72	0.12	0.164	2.411	0.965	2.73	1.17	0.39	72	-44	-112	2600.3	0.982	Nonordnance
FUS-48	64.93	139.90	0.08	64.87	139.98	0.18	0.032	0.017	0.780	1.52	0.00	0.07	3	-180	-151	419.8	0.938	Frag
FUS-49	73.51	120.40	0.07	73.65	120.42	0.06	0.048	0.061	0.988	1.08	0.13	0.50	-5	117	132	588.2	0.970	Nonordnance
FUS-50	67.23	118.92	0.08	67.31	118.89	0.08	0.102	0.574	0.987	0.74	0.05	0.06	14	112	156	381.9	0.937	No dig sheet
FUS-51	69.50	94.68	0.06	69.42	94.63	0.08	0.052	0.078	0.989	3.23	0.85	0.42	-1	177	-174	9141.3	0.925	Nonordnance
FUS-52	48.17	131.23	0.08	47.98	131.25	0.04	0.027	0.011	0.921	0.36	0.20	0.22	-29	-61	123	244.2	0.954	Frag
FUS-53	46.30	133.26	0.07	46.12	133.16	0.09	0.043	0.043	0.916	1.94	0.45	0.62	14	172	-87	2197.4	0.968	Frag
FUS-54	59.48	152.90	0.05	59.47	152.86	0.11	0.071	0.198	0.977	1.00	0.00	0.07	-1	107	177	452.4	0.921	Nonordnance
FUS-55	52.37	164.19	0.74	52.36	164.14	0.18	0.401	35.101	0.944	9.61	3.56	2.43	21	-148	-122	4393.8	0.978	Nonordnance
FUS-56	59.91	163.11	0.10	59.9	163.17	0.09	0.026	0.009	0.937	0.59	0.14	0.39	-7	-2	-49	198.8	0.979	Frag
FUS-57	57.82	168.13	0.57	57.84	168.07	0.50	0.091	0.415	0.977	4.91	2.82	2.23	61	-55	77	607.6	0.978	81-mm mortar
FUS-58	46.54	167.83	0.41	46.49	167.62	0.45	0.104	0.618	0.884	1.97	1.27	0.73	59	-160	32	170.8	0.960	Nonordnance
FUS-59	55.48	173.89	0.49	55.47	173.73	0.52	0.076	0.243	0.923	4.06	1.80	2.20	62	44	-90	218.5	0.971	81-mm mortar
FUS-60	37.47	170.69	0.56	37.37	170.89	0.69	0.076	0.238	0.912	6.00	2.17	3.38	-59	-37	-108	218.2	0.978	81-mm mortar
FUS-61	36.59	159.14	0.19	36.55	159.21	0.12	0.103	0.596	0.989	1.19	0.44	0.29	-32	77	-174	867.7	0.964	Frag
FUS-62	43.8	164.26	0.32	43.8	164.26	0.02			0.983	0.21	0.00	0.02	79	-52	3	230.7	0.983	Nothing found
FUS-63	51.45	40.57	0.45	51.45	40.63	0.38	0.077	0.243	0.980	5.27	1.12	0.59	33	84	-2	784.4	0.957	81-mm mortar seeded
FUS-64	77.37	58.42	0.79	76.96	58.67	0.51	0.118	0.886	0.947	11.95	3.27	3.21	8	143	177	1582.0	0.954	4.2" seeded
FUS-65	86.33	56.00	0.31	86.33	56.01	0.29	0.101	0.559	0.932	6.62	0.96	1.49	57	115	10	2315.9	0.987	25lb Frag bomb
FUS-66	86.19	52.41	0.30	86.1	52.46	0.26	0.047	0.058	0.980	2.86	0.26	0.94	3	15	-161	824.8	0.963	2.75" WH seeded
FUS-67	105.39	62.43	0.29	105.53	62.32	0.19	0.079	0.269	0.982	1.78	0.91	0.81	72	138	-118	2721.6	0.964	2.75" WH seeded
FUS-68	111.13	62.61	0.62	111.08	62.58	0.53	0.066	0.155	0.941	9.42	1.34	1.16	9	48	-101	431.7	0.927	81-mm mortar seeded
FUS-69	124.20	67.11	0.18	124.08	67.16	0.16	0.063	0.133	0.983	4.92	0.63	0.46	-41	32	-71	42666	0.821	MK23 seeded
FUS-70	129.70	73.13	0.10	129.61	73.19	0.04	0.036	0.025	0.967	0.44	0.33	0.41	-11	121	90	720.7	0.972	2.75" RktMtr/FinsOpen
FUS-71	68.85	71.70	0.14	68.89	71.66	0.10	0.066	0.155	0.944	3.92	1.43	1.85	-12	-163	-108	2747.3	0.978	81-mm mortar
FUS-72	182.05	103.38	0.26	182.14	103	0.37	0.083	0.307	0.811	11.79	2.38	3.67	32	-100	-13	8879.9	0.964	81-mm mortar

Appendix B. MTADS Target Report from the L Range Demonstration (continued).

Target #	Mag Local X (m)	Mag Local Y (m)	Mag Depth (m)	3β Local X (m)	3β Local Y (m)	3β EM Depth (m)	Mag Size (m)	Mag Moment	Fit Quality	β1	β2	β3	Theta	Phi	Psi	χ2	3β Coherence	Remediation Results
FUS-73	168.12	114.90	0.07	167.77	114.62	0.06	0.091	0.409	0.993	0.43	0.29	0.22	0	34	44	352.3	0.968	Frag
FUS-74	168.27	145.56	0.10	168.68	145.74	0.26	0.074	0.219	0.970	2.06	1.44	0.95	-6	176	154	1537.9	0.920	No dig sheet
FUS-75	151.38	155.44	0.11	151.41	155.67	0.14	0.037	0.028	0.957	0.69	0.49	0.53	-6	-180	10	1028.7	0.942	Bomb fuze
FUS-76	153.89	145.49	0.32	153.62	145.34	0.38	0.056	0.097	0.866	3.33	1.36	1.40	-11	36	178	776.0	0.950	Ordnance-related
FUS-77	153.21	158.10	0.30	153.29	157.32	0.19	0.087	0.363	0.945	1.26	0.19	0.50	13	-148	-141	307.1	0.970	Frag
FUS-78	133.95	187.04	0.44	133.95	187.04	0.14			0.986	8.95	2.97	4.95	10	26	79	7499.0	0.986	Nonordnance
FUS-79	133.94	191.98	0.37	133.63	191.89	0.44	0.073	0.213	0.956	5.64	1.76	2.82	40	-166	-114	1741.3	0.957	81-mm mortar
FUS-80	133.99	183	0.66	133.99	183	0.36			0.946	6.93	2.92	1.94	-21	-5	-152	2692.6	0.946	Nonordnance
FUS-81	129.53	190.78	0.08	129.33	190.8	0.08	0.080	0.280	0.969	0.34	0.26	0.06	-20	119	166	197.4	0.939	Frag
FUS-82	132.11	195.09	0.35	132.11	195.09	0.05			0.987	0.26	0.09	0.23	62	-11	-120	113.0	0.987	Nothing found
FUS-83	168.47	99.63	0.14	168.5	99.69	0.09	0.078	0.258	0.955	4.93	1.11	1.29	2	-113	-175	15748	0.953	Mortar
FUS-84	166.78	106.86	0.13	166.87	106.96	0.09	0.059	0.109	0.972	0.69	0.11	0.18	-82	158	4	868.2	0.981	Nonordnance
FUS-85	164.90	107.62	0.14	164.86	107.61	0.32	0.112	0.765	0.915	6.15	2.01	1.08	13	90	-160	3501.3	0.918	81-mmIII section
FUS-86	165.32	120.7	0.56	165.32	120.7	0.26			0.944	1.46	0.41	1.04	-25	113	-76	562.9	0.944	Frag
FUS-87	165.3	124.12	0.42	165.3	124.12	0.12			0.967	1.05	0.13	0.70	-24	124	170	1616.5	0.967	Frag
FUS-88	149.67	111.73	0.33	149.67	111.73	0.03			0.952	0.62	0.11	0.15	71	24	-69	2960.4	0.952	Ordnance-related
FUS-89	158.99	113.81	0.13	158.71	113.94	0.23	0.037	0.027	0.930	2.20	0.88	1.80	6	173	121	1199.2	0.963	Ordnance-related
FUS-90	157.74	117.69	0.21	158.11	117.53	0.37	0.042	0.040	0.902	2.26	2.04	0.45	20	-31	-24	1220.7	0.888	Frag
FUS-91	160.94	118.81	0.08	160.92	118.92	0.28	0.036	0.025	0.869	2.30	1.19	0.91	17	171	-83	2897.7	0.872	Ordnance-related
FUS-92	161.53	116.61	0.16	161.61	116.61	0.20	0.055	0.091	0.981	6.22	3.04	2.29	-5	-2	-5	6318.0	0.972	81-mm mortar
FUS-93	149.21	158.38	0.14	149.24	158.33	0.09	0.041	0.036	0.888	0.93	0.22	0.16	-15	13	-44	699.1	0.957	Frag
FUS-94	159.92	164.63	0.02	160.07	164.67	0.05	0.095	0.467	0.932	1.44	0.41	0.44	-9	135	137	1664.7	0.969	Frag
FUS-95	136.68	96.36	0.15	136.75	96.5	0.08	0.041	0.037	0.967	0.71	0.34	0.18	16	99	-137	848.1	0.920	2.75" RktMtr
FUS-96	136.14	101.52	0.08	136.07	101.48	0.17	0.059	0.112	0.915	5.67	3.00	2.67	-10	28	-124	7030.2	0.981	Recoilless rifle round 76-80-mm/18"
FUS-97	137.75	149.22	0.13	137.83	149.16	0.17	0.052	0.075	0.940	2.70	1.28	0.96	-12	100	175	4276.5	0.939	Ordnance-related
FUS-98	138.74	147.83	0.25	138.5	147.65	0.39	0.148	1.747	0.960	4.83	0.25	0.35	6	95	113	599.5	0.924	Frag
FUS-99	137.71	146.32	0.19	137.4	146.24	0.09	0.043	0.044	0.747	0.65	0.22	0.05	-62	-52	108	1862.2	0.958	Frag
FUS-100	138.32	143.45	0.32	138.55	143.38	0.27	0.045	0.048	0.619	1.59	0.38	1.02	33	17	-77	648.4	0.938	Ordnance-related
FUS-101	140.33	175.30	0.07	140.3	175.27	0.13	0.090	0.397	0.997	0.47	0.02	0.12	5	-165	110	155.9	0.888	Frag
FUS-102	133.83	171.49	0.09	134.22	172.19	0.23	0.059	0.113	0.933	1.14	0.56	1.10	11	85	-100	500.0	0.945	Frag
FUS-103	137.26	191.92	0.13	137.26	191.87	0.18	0.065	0.152	0.985	3.30	1.51	0.84	20	81	-168	2616.2	0.975	Nonordnance
FUS-104	138.56	191.62	0.20	138.33	191.7	0.24	0.036	0.026	0.948	2.51	0.93	1.42	-13	-3	170	2155.4	0.966	60-mm mortar
FUS-105	136.68	189.81	0.26	136.7	189.87	0.24	0.062	0.132	0.960	5.65	1.53	1.13	18	36	41	2210.2	0.986	81-mm mortar
FUS-106	132.99	85.46	0.28	132.97	85.37	0.28	0.100	0.539	0.992	1.15	0.18	0.00	-50	56	113	744.1	0.928	Frag
FUS-107	126.83	94.48	0.54	126.76	94.45	0.45	0.243	7.832	0.859	189.02	45.23	89.93	2	-178	-77	815158	0.918	5" Rkt
FUS-108	124.10	96.01	0.13	124.14	96.06	0.04	0.032	0.017	0.761	5.30	1.40	3.62	-45	119	127	71941	0.972	Nonordnance
FUS-109	130.87	112.16	0.40	131.36	112.59	0.07	0.110	0.728	0.693	7.47	1.98	2.02	-4	86	-47	21118.2	0.963	Frag

Appendix B. MTADS Target Report from the L Range Demonstration (continued).

Target #	Mag Local X (m)	Mag Local Y (m)	Mag Depth (m)	3β Local X (m)	3β Local Y (m)	3β EM Depth (m)	Mag Size (m)	Mag Moment	Fit Quality	β1	β2	β3	Theta	Phi	Psi	χ2	3β Coherence	Remediation Results
FUS-110	123.26	123.52	0.11	123.32	123.36	-0.01	0.041	0.036	0.940	0.25	0.15	0.20	9	-104	-123	451.4	0.950	Ordnance-related
FUS-111	129.01	123.99	0.21	128.91	124.09	0.16	0.072	0.200	0.922	0.92	0.20	0.73	5	130	-85	537.7	0.916	Frag
FUS-112	125.64	136.44	0.28	125.55	136.46	0.26	0.037	0.028	0.861	2.16	1.63	1.16	-55	101	-122	1391.3	0.980	81-mm mortar
FUS-113	128.76	136.30	0.11	128.69	136.25	0.10	0.042	0.041	0.925	0.47	0.34	0.26	-6	-10	-152	253.5	0.973	Nonordnance
FUS-114	123.54	162.86	0.22	123.5	162.74	0.17	0.103	0.585	0.936	4.18	0.65	0.56	1	72	-180	1404.7	0.966	Nonordnance
FUS-115	130.77	175.56	0.35	130.61	175.46	0.37	0.080	0.276	0.980	5.86	2.51	2.89	55	-163	117	1657.1	0.980	No dig sheet
FUS-116	122.95	175.89	0.08	122.84	175.9	0.27	0.040	0.035	0.986	3.75	0.57	0.31	2	-95	-9	1539.8	0.897	Nonordnance
FUS-117	119.33	166.90	0.44	119.51	166.9	0.37	0.087	0.352	0.958	7.60	2.00	3.20	33	-24	-143	6522.1	0.955	81-mm mortar
FUS-118	123.23	168.45	0.11	122.88	168.73	0.12	0.018	0.003	0.707	0.65	0.21	0.20	37	-124	-103	592.7	0.941	Frag
FUS-119	126.29	197.71	0.05	126.35	197.51	0.06	0.041	0.038	0.888	0.92	0.27	0.29	7	2	-46	427.6	0.965	Ordnance-related
FUS-120	133.84	204.27	0.09	133.88	204.32	0.11	0.051	0.074	0.968	0.58	0.38	0.28	41	165	120	398.5	0.970	Ordnance-related
FUS-121	113.27	78.31	0.17	113.62	78.29	0.27	0.061	0.122	0.877	1.77	0.33	0.20	1	-163	-12	340.4	0.905	Nonordnance
FUS-122	108.73	88.75	0.18	108.77	88.79	0.15	0.064	0.142	0.894	5.02	2.01	2.10	-3	57	-171	6490.4	0.979	81-mm mortar
FUS-123	111.67	100.19	0.11	111.51	100.22	0.13	0.087	0.355	0.902	0.84	0.26	0.48	-6	85	114	851.3	0.900	Frag
FUS-124	118.45	106.53	0.55	118.57	106.59	0.42	0.082	0.300	0.957	3.62	1.52	2.10	54	46	44	593.6	0.981	81-mm mortar
FUS-125	120.26	112.66	0.12	120.33	112.83	0.26	0.042	0.039	0.932	1.66	0.68	1.05	-7	-99	102	841.9	0.901	Ordnance-related
FUS-126	113.56	132.65	0.10	113.2	133.16	0.06	0.041	0.037	0.967	0.75	0.25	0.07	-73	43	-145	1025.2	0.976	Frag
FUS-127	106.36	134.57	0.11	106.34	134.66	0.22	0.084	0.321	0.792	1.08	0.05	0.06	-6	1	-56	387.6	0.868	Frag
FUS-128	120.67	135.58	0.11	120.66	135.43	0.34	0.064	0.143	0.910	3.05	0.04	0.16	-5	-110	1	802.8	0.859	Nonordnance
FUS-129	109.89	153.80	0.47	109.86	153.77	0.12	0.272	10.942	0.897	3.46	1.89	0.71	9	-121	101	4377.4	0.973	Nonordnance
FUS-130	111.49	163.56	0.27	111.42	163.58	0.18	0.066	0.153	0.983	4.57	1.83	1.35	-21	13	-50	2929.1	0.983	81-mm mortar
FUS-131	108.55	164.24	0.37	108.68	164.37	0.42	0.060	0.120	0.660	4.09	1.76	2.99	-44	126	-60	319.0	0.985	81-mm mortar
FUS-132	115.74	167.11	0.09	115.69	167.02	0.09	0.061	0.122	0.983	3.66	0.78	2.16	-5	-2	-107	5265.1	0.971	Nonordnance
FUS-133	89.84	190.89	0.10	89.7	190.91	0.13	0.082	0.299	0.985	1.26	0.61	0.41	5	74	0	776.5	0.954	60-mm mortar
FUS-134	88.15	184.29	0.06	88.15	184.31	-0.04	0.085	0.331	0.981	0.14	0.00	0.01	-7	-18	-38	51.9	0.926	Frag
FUS-135	91.05	177.83	0.04	91.11	177.85	0.06	0.049	0.063	0.984	1.46	0.70	0.27	8	-91	-17	660.7	0.978	Frag
FUS-136	91.11	175.62	0.12	90.88	175.14	0.06	0.071	0.198	0.957	0.28	0.10	0.23	27	66	127	281.1	0.959	Frag
FUS-137	93.82	174.63	0.59	93.88	174.45	0.27	0.337	20.752	0.956	4.66	1.31	2.46	34	-118	25	3925.3	0.961	Nonordnance
FUS-138	94.64	172.09	0.01	94.71	172.17	0.11	0.042	0.039	0.783	2.48	1.87	1.43	8	-87	-23	3358.2	0.968	81-mm nose section
FUS-139	96.03	178.16	0.24	95.25	177.14	0.30	0.095	0.466	0.703	5.31	2.14	1.29	8	-18	24	2296.5	0.933	Frag
FUS-140	101.05	171.69	0.25	100.98	171.81	0.22	0.154	1.983	0.988	17.28	9.43	13.14	-45	-24	-118	13596.3	0.968	Frag
FUS-141	94.33	158.52	0.13	94.35	158.42	0.17	0.075	0.227	0.981	0.93	0.35	0.22	44	-58	-1	1256.7	0.946	Frag
FUS-142	90.06	157.56	0.65	90.08	157.5	0.35	0.357	24.791	0.970	9.33	2.85	1.71	-4	-171	-72	1929.7	0.971	Nonordnance
FUS-143	86.70	157.14	0.30	86.81	157.39	0.30	0.084	0.317	0.986	6.46	1.98	0.91	-42	-124	138	1979.0	0.985	81-mm mortar
FUS-144	92.85	157.30	0.11	92.71	156.53	0.02	0.064	0.143	0.917	0.47	0.02	0.07	47	-88	148	1563.3	0.948	Frag
FUS-145	96.22	151.97	0.53	96.08	152.07	0.30	0.329	19.350	0.977	10.73	2.71	3.75	10	-36	166	3283.4	0.970	Nonordnance
FUS-146	94.98	119.88	0.42	94.88	119.51	0.63	0.058	0.104	0.893	14.51	3.98	1.43	30	-86	34	3184.2	0.929	81-mm mortar

Appendix B. MTADS Target Report from the L Range Demonstration (continued).

Target #	Mag Local X (m)	Mag Local Y (m)	Mag Depth (m)	3β Local X (m)	3β Local Y (m)	3β EM Depth (m)	Mag Size (m)	Mag Moment	Fit Quality	β1	β2	β3	Theta	Phi	Psi	χ2	3β Coherence	Remediation Results
FUS-147	96.13	122.24	0.09	96.07	122.16	0.15	0.050	0.066	0.836	2.94	1.20	2.03	12	-59	-68	5986.2	0.911	Bomb fuze
FUS-148	91.29	117.57	0.75	90.92	117.31	0.98	0.130	1.187	0.968	48.84	14.22	6.10	27	-115	-133	1096.4	0.948	105-mm plus scrap
FUS-149	95.12	115.82	0.20	94.66	115.95	0.14	0.049	0.066	0.800	0.73	0.14	0.33	63	-172	-68	996.4	0.963	Frag
FUS-150	97.11	109.69	0.29	97.11	109.74	0.34	0.075	0.226	0.875	3.89	2.26	3.27	16	121	109	2661.4	0.943	4.2" broke in half
FUS-151	97.63	94.70	0.02	97.54	94.72	0.07	0.057	0.098	0.850	4.45	1.42	1.69	10	62	126	9741.1	0.967	Frag
FUS-152	105.68	90.28	0.08	105.17	90.29	0.05	0.108	0.688	0.974	1.25	0.84	1.00	69	-7	-48	3833.6	0.971	Frag
FUS-153	92.88	72.93	0.22	92.89	72.68	0.29	0.078	0.257	0.829	3.76	2.15	2.03	30	12	66	1540.5	0.978	81-mm mortar
FUS-154	78.77	71.03	0.10	78.85	71.06	0.01	0.074	0.224	0.907	6.10	2.61	1.76	9	-97	-154	22986.3	0.984	81-mm Illum
FUS-155	81.02	76.06	0.19	81.05	76.19	0.19	0.083	0.315	0.943	4.66	2.28	1.41	42	33	170	11688.7	0.958	81-mm mortar
FUS-156	74.53	70.36	0.21	74.59	70.29	0.23	0.062	0.132	0.953	6.79	3.69	2.35	4	167	16	15916.3	0.925	81-mm mortar
FUS-157	76.18	72.49	0.09	76.16	72.55	0.12	0.045	0.049	0.977	3.20	1.44	0.60	1	54	-161	5657.4	0.936	Frag
FUS-158	84.51	86.96	0.17	84.59	86.91	0.13	0.032	0.018	0.964	2.01	0.51	0.86	-3	141	-91	1186.9	0.969	Frag
FUS-159	82.38	118.97	0.48	82.28	118.92	0.42	0.085	0.333	0.948	3.71	2.02	2.44	-52	9	92	654.3	0.983	81-mm mortar
FUS-160	79.13	114.53	0.45	78.86	114.35	0.47	0.070	0.186	0.906	5.17	1.93	2.60	43	-92	-93	1499.7	0.962	81-mm mortar
FUS-161	83.50	142.28	0.56	83.71	142.17	0.43	0.085	0.330	0.967	7.97	2.09	3.22	27	-12	58	2417.7	0.954	81-mm mortar
FUS-162	77.86	167.73	0.35	77.86	167.73	0.05			0.977	0.28	0.19	0.25	35	-128	160	164.6	0.977	Ordnance-related
FUS-163	75.37	173.65	0.12	75.3	173.86	0.05	0.045	0.049	0.827	0.86	0.54	0.70	16	55	44	803.8	0.976	Ordnance-related
FUS-164	83.62	173.63	0.78	83.95	173.19	0.86	0.332	19.820	0.886	41.23	0.00	40.33	-42	-116	44	10115.4	0.926	Nonordnance
FUS-165	74.88	182.53	0.64	74.73	182.7	0.41	0.073	0.212	0.905	3.91	0.53	1.62	8	-111	-10	1346.3	0.907	81-mm mortar
FUS-166	74.38	187.01	0.45	74.48	187.21	0.69	0.088	0.366	0.981	3.45	1.68	1.61	71	26	85	723.0	0.985	81-mm mortar
FUS-167	81.47	186.46	0.42	81.82	186.88	0.65	0.055	0.092	0.947	10.54	3.16	1.69	9	49	-58	695.7	0.915	81-mm mortar
FUS-168	83.42	188.39	0.55	83.52	188.68	0.84	0.293	13.672	0.941	28.63	2.85	0.00	54	45	122	11281.8	0.889	Nonordnance
FUS-169	63.84	185.26	0.56	63.88	185.31	0.47	0.077	0.250	0.973	2.85	1.98	1.57	59	-70	-56	240.6	0.989	81-mm mortar
FUS-170	64.40	183.25	0.38	64.39	183.12	0.42	0.067	0.165	0.950	7.23	2.62	2.11	26	-74	49	1755.0	0.970	81-mm mortar
FUS-171	66.42	182.07	0.51	66.75	182.18	0.75	0.073	0.215	0.981	4.80	0.78	1.53	35	151	114	314.0	0.969	81-mm mortar
FUS-172	58.50	170.57	0.25	60.68	170.58	0.58	0.244	7.842	0.772	8.29	3.11	2.13	-30	175	-148	592.3	0.967	Frag
FUS-173	62.97	170.42	0.09	62.96	170.35	0.11	0.124	1.026	0.731	3.94	1.13	0.54	-6	-127	155	1957.3	0.978	Frag
FUS-174	67.74	168.10	0.48	67.6	167.98	0.37	0.112	0.769	0.950	8.08	2.41	4.68	36	-117	-164	2574.6	0.983	81-mm mortar
FUS-175	65.69	157.17	0.04	65.65	157.21	0.11	0.036	0.025	0.792	0.97	0.73	0.55	12	99	174	1076.1	0.966	Frag
FUS-176	71.00	159.89	0.33	71.37	159.62	0.47	0.070	0.185	0.962	5.60	2.19	1.69	30	-51	-137	823.1	0.976	Frag
FUS-177	60.18	151.02	0.01	60.19	151	0.02	0.039	0.033	0.994	0.74	0.11	0.07	-3	-149	-177	752.4	0.945	Nonordnance
FUS-178	61.22	130.56	0.59	61.15	129.97	0.93	0.080	0.283	0.943	4.90	1.20	4.28	68	-122	-179	357.0	0.971	81-mm mortar
FUS-179	63.00	127.23	0.16	63.1	127.31	0.11	0.068	0.171	0.972	0.58	0.05	0.24	50	121	-159	960.4	0.957	Frag
FUS-180	60.93	116.11	0.63	60.8	116.24	0.40	0.098	0.512	0.947	3.97	2.37	1.20	23	124	-124	957.8	0.971	81-mm mortar
FUS-181	67.45	88.93	1.17	67.98	89.09	1.17	0.180	3.157	0.948	168.06	60.27	52.22	-6	32	-144	4173.4	0.931	8 Venturies
FUS-182	70.63	88.05	0.15	70.68	88.08	0.13	0.071	0.193	0.967	7.11	2.96	2.39	-6	-114	22	26947.1	0.949	81-mm mortar
FUS-183	71.12	85.62	0.37	71.09	85.64	0.36	0.270	10.704	0.846	106.81	11.72	31.51	-4	58	-6	914831.	0.869	Nonordnance

Appendix B. MTADS Target Report from the L Range Demonstration (continued).

Target #	Mag Local X (m)	Mag Local Y (m)	Mag Depth (m)	3β Local X (m)	3β Local Y (m)	3β EM Depth (m)	Mag Size (m)	Mag Moment	Fit Quality	β1	β2	β3	Theta	Phi	Psi	χ ²	3β Coherence	Remediation Results
FUS-184	75.91	86.17	0.40	75.57	86.52	0.68	0.115	0.830	0.888	10.69	6.42	9.08	40	21	-97	1177.4	0.968	Frag
FUS-185	77.42	84.72	0.45	77.59	84.75	0.20	0.121	0.955	0.763	10.73	4.40	8.30	9	80	-101	42512.9	0.945	81-mm mortar
FUS-186	55.71	132.81	0.48	55.28	132.81	0.39	0.086	0.342	0.917	5.59	1.98	1.45	50	-154	106	1419.2	0.983	81-mm mortar
FUS-187	45.62	146.87	0.14	45.69	146.82	0.07	0.067	0.163	0.981	5.24	1.04	1.68	-13	132	-128	42751.7	0.922	Nonordnance
FUS-188	55.82	143.67	0.77	55.72	143.8	0.47	0.125	1.067	0.951	5.69	4.06	2.07	63	93	-20	999.3	0.978	15-25 frag bomb
FUS-189	54.79	150.73	0.42	54.86	150.67	0.34	0.089	0.383	0.977	6.32	2.48	1.51	40	-5	29	7431.4	0.948	81-mm mortar
FUS-190	50.89	140.98	0.12	50.77	141.02	0.15	0.029	0.014	0.838	1.39	0.37	0.49	0	-2	-129	457.5	0.966	Nonordnance
FUS-191	46.75	159.70	0.17	46.77	159.72	0.10	0.103	0.593	0.975	0.74	0.13	0.26	17	125	-96	227.4	0.957	Frag
FUS-192	51.15	179.35	0.50	51.31	179.58	0.43	0.077	0.249	0.936	4.91	1.90	2.21	15	38	-171	381.0	0.984	81-mm mortar
FUS-193	50.45	170.94	0.57	50.45	170.94	0.27			0.981	2.06	0.62	0.91	36	2	22	195.3	0.981	60-mm M720
FUS-194	44.21	175.55	0.60	44.13	175.3	0.52	0.074	0.217	0.957	3.96	0.50	1.73	42	-46	172	612.2	0.954	81-mm HE M371
FUS-195	45.83	172.30	0.55	45.71	172.28	0.53	0.073	0.214	0.961	3.13	1.47	2.59	-49	149	-170	342.4	0.974	81-mm mortar
FUS-196	40.04	176.63	0.07	40.01	176.76	0.21	0.036	0.025	0.798	2.61	1.17	1.63	11	-35	66	1977.6	0.967	Frag
FUS-197	35.78	175.99	0.36	35.87	176.09	0.50	0.061	0.124	0.928	5.57	3.77	2.31	37	-2	-31	604.1	0.975	81-mm mortar
FUS-198	29.47	176.71	0.33	29.59	176.63	0.37	0.057	0.101	0.958	5.90	2.84	4.43	-26	146	-91	1589.6	0.978	81-mm mortar
FUS-199	41.30	51.76	0.45	41.38	51.93	0.71	0.085	0.331	0.959	14.02	2.06	5.82	61	-20	166	9362.6	0.817	81-mm mortar
FUS-200	49.44	48.31	0.17	49.43	48.45	0.23	0.050	0.066	0.939	4.02	0.34	0.66	-2	-78	-116	1604.4	0.931	MK23 seeded
FUS-201	90.08	67.30	0.82	90.01	67.52	0.56	0.115	0.828	0.979	5.85	1.61	4.69	6	154	-32	1296.1	0.946	105-mm seeded

APPENDIX C

MTADS TARGET REPORT FROM THE BBR IMPACT AREA DEMONSTRATION

This page left blank intentionally.

Table C-1. Model Results for 105-mm Projectiles.

ID	Magnetometer Fit									3- β Fit										
	Local X (m)	Local Y (m)	Depth (m)	Size (m)	Inclin.	Az.	Fit Qual.	Comments	Cat.	Local X (m)	Local Y (m)	Depth (m)	Θ	Φ	Ψ	β_1	β_2	β_3	Fit Qual.	χ^2
13	389.49	548.04	0.66	0.125	71	261	0.952	poor degaussing, 105, nose down	2	389.44	547.73	0.35	-37	61	-47	12.1	4.2	5.9	0.981	8373
59	538.57	579.57	0.74	0.147	82	170	0.975	good fit for a 155	1	538.61	579.46	0.45	46	-139	-15	10.0	7.0	3.8	0.972	3567
99	507.18	585.20	0.91	0.141	74	222	0.969	105, nose down	1	507.06	584.88	0.60	28	-106	122	9.2	3.1	0.0	0.938	2189
133	474.58	656.87	0.67	0.117	55	251	0.960	105, slight remnant	2	474.67	656.84	0.37	24	47	-26	8.4	3.5	6.6	0.989	4528
142	512.94	679.83	0.61	0.101	34	30	0.954	105mm	1	512.92	679.85	0.31	-13	50	-125	8.4	5.2	6.5	0.980	6308
149	460.22	689.48	0.69	0.138	51	312	0.982	105/155mm, E/W, nose down	1	460.41	689.39	0.37	65	-51	-112	6.4	4.4	5.6	0.977	2063
163	434.35	711.40	0.67	0.135	47	299	0.972	155mm, E/W	1	434.40	711.43	0.62	9	138	160	6.5	4.2	5.5	0.979	6577

ID	Constrained 3- β Fit											S_1 (max)
	Local X (m)	Local Y (m)	Depth (m)	Θ	Φ	Ψ	β_1	β_2	β_3	Fit Qual.	χ^2	
13	389.52	547.88	0.53	88	42	46	16.8	11.8	11.8	0.966	15046	2859
59	538.74	579.55	0.46	73	-60	-175	8.8	5.1	5.1	0.968	4368	1680
99	507.05	585.24	0.77	81	-127	-150	8.8	5.1	5.1	0.919	3636	626
133	474.52	656.78	0.42	62	-129	-168	8.8	5.1	5.1	0.969	13215	3222
142	512.98	679.88	0.53	79	154	-54	16.8	11.8	11.8	0.965	11233	2432
149	460.39	689.41	0.63	87	-1	-162	16.8	11.8	11.8	0.959	4566	1697
163	434.39	711.39	0.89	85	95	133	16.8	11.8	11.8	0.968	11265	1913

Table C-2. Model Results for 155-mm Projectiles.

ID	Magnetometer Fit									3- β Fit										
	Local X (m)	Local Y (m)	Depth (m)	Size (m)	Inclin.	Az.	Fit Qual.	Comments	Cat.	Local X (m)	Local Y (m)	Depth (m)	Θ	Φ	Ψ	β_1	β_2	β_3	Fit Qual.	χ^2
86	383.80	601.67	0.73	0.217	-69	282	0.950	totally inverted, fence post	5	383.82	601.68	0.33	26	-111	-71	18.7	12.3	16.0	0.985	21187
88	429.63	581.65	0.86	0.204	75	355	0.947	good fit for 8in	1	429.67	581.65	0.43	15	-27	21	14.0	11.2	8.8	0.984	4818
104	539.83	624.56	0.85	0.164	31	28	0.974	155mm	1	539.95	624.51	0.43	5	-149	139	14.1	11.6	10.4	0.989	4608
109	482.37	621.69	1.12	0.209	72	270	0.956	8-in, E/W	1	481.80	621.61	0.89	-23	-16	24	55.0	37.0	15.2	0.903	3469
121	367.38	636.27	0.92	0.092	44	4	0.867	Clutter	6	367.60	635.55	0.46	11	-64	-119	6.0	2.4	1.3	0.889	2699
132	441.28	657.90	0.57	0.132	45	316	0.983	likely 105	1	441.20	657.91	0.51	-31	-25	-120	17.4	12.7	15.4	0.993	9137
135	500.78	651.99	1.03	0.133	69	54	0.874	105mm, nose down	1	500.70	651.86	0.64	37	-118	-166	19.8	10.9	14.6	0.986	2561
148	468.05	683.84	0.81	0.156	63	188	0.986	155mm	1	467.91	683.72	0.53	-9	-23	-167	25.8	8.4	15.3	0.984	10862
154	394.32	691.49	1.39	0.235	87	3	0.941	deep 8-in, nose down	1	394.14	691.43	1.05	-11	42	-77	23.6	9.5	4.3	0.913	2354
167	502.18	717.05	1.04	0.108	64	359	0.921	possible deep 105mm	2	502.10	716.87	1.00	1	17	-20	53.8	6.9	32.5	0.930	2239

ID	Constrained 3- β Fit											S_1 (max)
	Local X (m)	Local Y (m)	Depth (m)	Θ	Φ	Ψ	β_1	β_2	β_3	Fit Qual.	χ^2	
86	383.79	601.77	0.57	71	157	53	40.6	28.8	28.8	0.973	38105	4482
88	429.69	581.67	0.49	20	-27	-78	16.8	11.8	11.8	0.982	5248	1984
104	540.02	624.56	0.47	29	22	-4	16.8	11.8	11.8	0.986	5893	2405
109	481.95	621.85	0.70	16	123	-95	16.8	11.8	11.8	0.871	6584	901
121	367.52	635.82	0.75	77	145	172	8.8	5.1	5.1	0.755	5386	599
132	441.19	657.90	0.48	-45	-40	50	16.8	11.8	11.8	0.987	15631	5917
135	500.78	652.02	0.59	39	55	43	16.8	11.8	11.8	0.983	3052	1666
148	467.87	683.65	0.29	5	175	54	8.8	5.1	5.1	0.954	33511	3279
154	394.27	691.45	0.86	-8	35	149	8.8	5.1	5.1	0.862	3746	631
167	502.26	717.06	1.00	14	39	32	40.6	28.8	28.8	0.877	4311	854

Table C-3. Model Results for 8-in Projectiles.

Magnetometer Fit										3- β Fit										
ID	Local X (m)	Local Y (m)	Depth (m)	Size (m)	Inclin.	Az.	Fit Qual.	Comments	Cat.	Local X (m)	Local Y (m)	Depth (m)	Θ	Φ	Ψ	β_1	β_2	β_3	Fit Qual.	χ^2
26	470.81	534.05	1.12	0.166	88	147	0.942	likely 155, nose down	1	470.92	534.06	0.66	25	12	-58	33.6	25.9	20.4	0.975	7905
89	415.36	597.87	0.76	0.192	29	15	0.962	155mm/8in, good target	1	415.33	597.83	0.41	39	-152	-108	43.0	33.1	35.9	0.993	17584
112	455.59	632.93	1.37	0.225	84	254	0.969	8-in deep	1	455.50	633.02	0.85	7	153	22	34.9	21.7	12.1	0.942	1726
139	538.84	657.89	1.12	0.210	70	84	0.981	8-in, E/W	1	538.99	657.88	0.74	32	72	57	37.1	28.0	28.6	0.981	3808
153	405.62	686.54	1.24	0.148	90	356	0.970	probable deep 155	1	405.50	686.62	0.88	10	90	8	10.2	6.5	3.5	0.919	2374

Constrained 3- β Fit												S_1 (max)
ID	Local X (m)	Local Y (m)	Depth (m)	Θ	Φ	Ψ	β_1	β_2	β_3	Fit Qual.	χ^2	
26	470.96	534.03	0.73	41	18	-116	40.6	28.8	28.8	0.974	8554	2513
89	415.30	597.82	0.38	30	-145	73	40.6	28.8	28.8	0.992	19930	9027
112	455.67	632.84	1.01	10	-44	-113	40.6	28.8	28.8	0.886	3391	646
139	539.00	657.90	0.75	35	71	54	40.6	28.8	28.8	0.981	3799	1965
153	405.47	686.57	1.13	7	93	-138	16.8	11.8	11.8	0.893	3024	603

Table C-4. Model Results for Frag Clusters.

ID	Magnetometer Fit									3- β Fit										
	Local X (m)	Local Y (m)	Depth (m)	Size (m)	Inclin.	Az.	Fit Qual.	Comments	Cat.	Local X (m)	Local Y (m)	Depth (m)	Θ	Φ	Ψ	β_1	β_2	β_3	Fit Qual.	χ^2
12	387.73	542.56	1.15	0.12	59	67	0.766	clutter pile	6	387.32	542.83	0.77	6	88	176	34.8	24.4	10.6	0.917	4292
21	448.97	546.51	1.06	0.109	63	121	0.745	low probability 105	3	448.62	547.19	0.41	-6	-87	-65	9.9	2.8	4.1	0.861	6280
24	454.15	532.88	0.84	0.087	81	46	0.645	low probability 105	3	454.15	533.20	0.31	5	145	-180	5.5	3.5	0.8	0.915	2266
25	460.18	531.62	0.87	0.102	39	48	0.852	possible 105	2	460.06	531.89	0.28	-3	30	179	2.9	1.8	0.8	0.874	3804
27	467.59	538.91	0.77	0.114	34	193	0.799	possible 105	3	466.79	539.08	0.66	-10	165	-91	65.0	2.2	30.2	0.815	12298
28	477.95	547.73	1.10	0.148	25	39	0.642	likely clutter pile	5	477.76	547.74	0.87	7	-12	85	87.8	21.0	44.3	0.897	8581
31	482.95	551.70	0.94	0.094	75	90	0.825	likely clutter	6	483.23	551.89	0.60	-5	52	127	14.8	6.2	0.0	0.893	3448
32	484.79	546.70	1.12	0.111	54	64	0.859	clutter	6	484.52	547.61	0.57	-5	78	169	14.6	7.9	1.8	0.902	3099
33	489.32	544.21	1.26	0.116	79	31	0.769	clutter	6	489.27	544.54	0.62	1	-107	99	16.9	5.3	11.8	0.883	2997
35	507.54	530.73	1.10	0.121	48	43	0.706	clutter	6	507.21	530.71	0.65	-3	-114	-64	30.8	9.4	15.3	0.809	22536
55	558.03	550.36	0.59	0.08	59	320	0.895	small end of a 105	3	557.51	550.38	0.58	4	-178	-163	26.5	17.8	4.0	0.868	13330
56	560.78	554.52	0.76	0.097	55	346	0.902	possible 105, 22 ft E of site	3	560.54	554.86	0.69	21	72	85	21.5	5.9	15.8	0.773	10249
66	479.21	563.93	0.80	0.091	65	35	0.881	possible 105	3	479.20	564.03	0.29	0	50	-79	4.3	1.3	2.2	0.942	2789
78	433.75	567.27	0.66	0.071	48	62	0.881	unlikely UXO	5	433.39	567.57	0.54	3	99	7	9.1	7.2	2.3	0.754	3875
134	495.47	643.93	0.65	0.097	46	58	0.892	low probability 105	3	495.37	643.96	0.43	22	14	-3	10.3	8.9	1.9	0.885	9076
150	447.43	675.04	1.20	0.147	89	105	0.887	possible deep 155	2	447.38	675.30	0.83	-5	-21	87	17.9	5.0	11.0	0.942	3722
157	364.18	729.66	0.84	0.123	79	65	0.897	possible 105 on N border	3	364.21	730.09	0.68	4	114	-176	11.5	7.7	1.3	0.900	6656
159	377.14	704.99	0.88	0.11	47	38	0.881	low probability 105	3	376.96	704.91	0.79	-2	101	176	7.9	6.1	1.7	0.893	3906
162	409.94	719.57	1.16	0.121	36	45	0.880	likely not UXO	4	409.94	719.60	0.98	4	-14	178	19.9	15.1	3.9	0.872	3258

ID	Constrained 3- β Fit											S_1 (max)
	Local X (m)	Local Y (m)	Depth (m)	Θ	Φ	Ψ	β_1	β_2	β_3	Fit Qual.	χ^2	
12	387.40	542.78	0.70	2	80	-96	16.8	11.8	11.8	0.838	9194	832
21	448.68	547.22	0.48	12	93	9	8.8	5.1	5.1	0.792	9094	758
24	454.17	533.23	0.56	-13	-35	-38	8.8	5.1	5.1	0.767	5733	504
25	460.25	531.98	0.66	15	8	137	8.8	5.1	5.1	0.791	6084	489
27	467.59	539.03	0.51	11	92	-104	8.8	5.1	5.1	0.696	20294	995
28	477.49	547.82	0.82	30	-24	-75	40.6	28.8	28.8	0.729	46798	1279
31	483.19	551.90	0.54	30	-134	38	8.8	5.1	5.1	0.803	5701	539

Table C-4. Model Results for Frag Clusters (continued).

ID	Local X (m)	Local Y (m)	Depth (m)	Θ	Φ	Ψ	β_1	β_2	β_3	Fit Qual.	χ^2	S_1 (max)
32	484.74	547.99	0.86	11	110	68	16.8	11.8	11.8	0.681	9715	707
33	489.36	544.57	0.53	-1	62	-120	8.8	5.1	5.1	0.784	6952	609
35	507.29	530.62	0.86	11	87	-172	40.6	28.8	28.8	0.752	29891	1262
55	557.92	550.29	0.98	19	40	150	40.6	28.8	28.8	0.744	24309	1012
56	560.56	554.75	0.99	33	59	-86	40.6	28.8	28.8	0.738	12279	992
66	479.19	564.10	0.55	3	56	49	8.8	5.1	5.1	0.898	4835	750
78	433.43	567.29	0.92	24	-25	157	16.8	11.8	11.8	0.585	6350	421
134	495.12	643.89	0.45	3	103	-73	8.8	5.1	5.1	0.806	16835	1165
150	447.42	675.35	1.27	22	125	103	40.6	28.8	28.8	0.881	7550	926
157	364.17	729.99	0.91	6	130	-39	16.8	11.8	11.8	0.809	12025	937
159	377.02	704.88	0.95	-12	93	91	8.8	5.1	5.1	0.778	6759	548
162	409.91	719.61	1.09	15	-36	-77	16.8	11.8	11.8	0.719	9710	514

Table C-5. Model Results for Frag Singles.

ID	Magnetometer Fit									3- β Fit										
	Local X (m)	Local Y (m)	Depth (m)	Size (m)	Inclin.	Az.	Fit Qual.	Comments	Cat.	Local X (m)	Local Y (m)	Depth (m)	Θ	Φ	Ψ	β_1	β_2	β_3	Fit Qual.	χ^2
29	479.96	541.89	0.38	0.065	34	54	0.980	too small for 105	6	480.08	541.83	-0.05	35	24	-99	0.5	0.1	0.0	0.925	5375
38	519.79	531.82	0.79	0.098	41	5	0.721	possible 105 in clutter	3	520.00	531.59	0.26	34	87	-42	2.1	1.3	1.6	0.879	7960
54	556.80	549.73	0.37	0.077	68	14	0.911	small end of 105	3	556.83	549.95	0.41	-21	-96	-6	13.4	9.8	3.9	0.928	14276
93	415.39	592.89	1.14	0.113	87	219	0.883	unlikely 105	3	415.11	593.38	0.37	0	-29	-98	9.4	1.9	5.9	0.879	8059
95	440.20	583.48	0.42	0.060	39	4	0.753	too small	6	440.05	583.58	0.00	23	97	-68	0.9	0.4	0.0	0.955	2865
98	481.95	600.68	0.49	0.060	48	356	0.856	too small	6	481.99	600.52	0.02	-13	25	178	1.1	0.1	0.3	0.884	2843
101	551.01	585.66	0.73	0.090	22	12	0.904	possible 105	2	551.05	586.08	0.46	-6	69	142	11.8	2.7	0.9	0.905	4129
107	480.20	634.17	1.00	0.121	35	14	0.892	possible 105	2	479.82	634.16	0.69	0	-122	-17	28.1	17.4	5.5	0.814	6592
128	402.60	649.59	0.94	0.104	74	224	0.905	multiple targets	5	402.74	649.98	0.70	-5	-48	66	22.6	4.7	14.9	0.901	3226
130	430.05	664.55	0.35	0.047	89	70	0.831	too small	6	429.97	664.41	0.20	-49	79	54	1.5	0.1	0.6	0.981	860
140	561.99	655.22	0.37	0.066	80	226	0.952	too small, outside site	6	562.37	654.95	0.22	-30	124	48	3.5	0.0	0.0	0.916	5830
143	507.27	686.48	0.36	0.049	45	1	0.797	trash	6	507.24	686.51	0.12	-41	-51	-153	1.3	0.1	0.2	0.958	2204

ID	Constrained 3- β Fit											S_1 (max)
	Local X (m)	Local Y (m)	Depth (m)	Θ	Φ	Ψ	β_1	β_2	β_3	Fit Qual.	χ^2	
29	480.19	541.63	0.75	77	57	-161	8.8	5.1	5.1	0.651	23975	712
38	519.98	531.55	0.66	85	-9	140	8.8	5.1	5.1	0.868	9583	743
54	556.79	549.84	0.55	22	95	148	16.8	11.8	11.8	0.878	24210	1913
93	415.11	593.24	0.69	-3	130	68	16.8	11.8	11.8	0.799	12420	753
95	440.12	583.49	0.73	70	65	-175	8.8	5.1	5.1	0.674	22434	687
98	482.26	600.34	0.60	46	-146	1	8.8	5.1	5.1	0.658	9234	559
101	551.15	586.29	0.58	-21	69	-111	8.8	5.1	5.1	0.707	11760	774
107	479.86	634.26	0.69	8	99	-85	16.8	11.8	11.8	0.627	18173	798
128	402.72	649.68	0.77	-2	-20	-125	16.8	11.8	11.8	0.839	6128	704
130	430.17	664.65	0.70	79	-138	59	8.8	5.1	5.1	0.828	10019	815
140	562.09	655.27	0.68	64	-77	61	8.8	5.1	5.1	0.642	26640	882
143	507.40	686.28	0.78	90	-158	-171	8.8	5.1	5.1	0.688	21227	860

Table C-6. Model Results for Clutter.

ID	Magnetometer Fit										3- β Fit										
	Local X (m)	Local Y (m)	Depth (m)	Size (m)	Inclin.	Az.	Fit Qual.	Comments	Cat.	Local X (m)	Local Y (m)	Depth (m)	Θ	Φ	Ψ	β_1	β_2	β_3	Fit Qual.	χ^2	
47	541.64	534.72	0.96	0.158	73	306	0.845	155 or 8 in deep, large clutter on top	2	541.96	535.37	0.59	-8	33	82	52.8	15.7	36.2	0.894	49779	
48	544.28	535.12	0.35	0.074	5	25	0.941	likely clutter	5	544.82	534.90	0.33	-7	95	-176	14.3	8.8	2.9	0.678	133241	
90	431.30	595.78	0.37	0.095	14	43	0.919	shallow 105	1	431.34	595.81	0.08	12	49	97	4.2	0.7	1.4	0.973	5382	
94	435.97	588.71	0.38	0.055	11	52	0.940	trash	6	436.09	588.58	0.03	7	24	25	1.1	0.2	0.0	0.915	2819	
116	413.49	616.89	0.38	0.085	17	350	0.957	low end of 105mm	1	413.58	616.90	0.10	4	101	23	4.4	0.1	1.2	0.967	7980	
168	523.52	700.80	0.33	0.084	24	30	0.936	possible shallow 105mm	2	523.50	700.83	0.06	-52	11	-96	3.7	1.1	2.5	0.984	9203	

ID	Constrained 3- β Fit											S_1 (max)
	Local X (m)	Local Y (m)	Depth (m)	Θ	Φ	Ψ	β_1	β_2	β_3	Fit Qual.	χ^2	
47	542.11	535.43	0.62	13	29	-147	40.6	28.8	28.8	0.826	98513	3231
48	544.81	534.91	0.72	-5	112	-173	40.6	28.8	28.8	0.587	168772	2044
90	431.29	595.73	0.36	2	38	-40	8.8	5.1	5.1	0.758	52957	1770
94	436.05	588.54	0.65	8	19	134	8.8	5.1	5.1	0.412	19932	674
116	413.74	616.87	0.49	86	106	160	8.8	5.1	5.1	0.673	78485	1869
168	523.61	700.90	0.26	-63	-122	-151	8.8	5.1	5.1	0.955	26602	4058



ESTCP Program Office

**901 North Stuart Street
Suite 303
Arlington, Virginia 22203**

**(703) 696-2117 (Phone)
(703) 696-2114 (Fax)**

**e-mail: estcp@estcp.org
www.estcp.org**